Free Radical Biology and Medicine 161 (2020) 32–49

Contents lists available at ScienceDirect

Free Radical Biology and Medicine

journal homepage: www.elsevier.com/locate/freeradbiomed

Original article

The molecular and physiological consequences of cold plasma treatment in murine skin and its barrier function

Anke Schmidt[a], Grit Liebelt[a,1], Johanna Striesow[a,1], Eric Freund[a,b], Thomas von Woedtke[a,c], Kristian Wende[a], Sander Bekeschus[a,*]

[a] Plasma Life Science and ZIK Plasmatis, Leibniz Institute for Plasma Science and Technology (INP), Felix-Hausdorff-Str. 2, 17489, Greifswald, Germany
[b] Department of General Visceral, Thoracic, and Vascular Surgery, Greifswald University Medical Center, Sauerbruchstr. DZ7, 17475, Greifswald, Germany
[c] Institute for Hygiene and Environmental Medicine, Greifswald University Medical Center, Sauerbruchstr., 17489, Greifswald, Germany

ARTICLE INFO

Keywords:
Lipidomics
Plasma medicine
Reactive oxygen and nitrogen species
Skin barrier
Transcriptomics

ABSTRACT

Cold plasma technology is an emerging tool facilitating the spatially controlled delivery of a multitude of reactive species (ROS) to the skin. While the therapeutic efficacy of plasma treatment has been observed in several types of diseases, the fundamental consequences of plasma-derived ROS on skin physiology remain unknown. We aimed to bridge this gap since the epidermal skin barrier and perfusion plays a vital role in health and disease by maintaining homeostasis and protecting from environmental damage. The intact skin of SKH1 mice was plasma-treated *in vivo*. Gene and protein expression was analyzed utilizing transcriptomics, qPCR, and Western blot. Immunofluorescence aided the analysis of percutaneous skin penetration of curcumin. Tissue oxygenation, perfusion, hemoglobin, and water index was investigated using hyperspectral imaging. Reversed-phase liquid-chromatography/mass spectrometry was performed for the identification of changes in the lipid composition and oxidation. Transcriptomic analysis of plasma-treated skin revealed modulation of genes involved in regulating the junctional network (tight, adherence, and gap junctions), which was confirmed using qPCR, Western blot, and immunofluorescence imaging. Plasma treatment increased the disaggregation of cells in the *stratum corneum* (SC) concomitant with increased tissue oxygenation, gap junctional intercellular communication, and penetration of the model drug curcumin into the SC preceded by altered oxidation of skin lipids and their composition *in vivo*. In summary, plasma-derived ROS modify the junctional network, which promoted tissue oxygenation, oxidation of SC-lipids, and restricted penetration of the model drug curcumin, implicating that plasma may provide a novel and sensitive tool of skin barrier regulation.

1. Introduction

The skin protects against detrimental dehydration, temperature variations, infection, and biological factors acting as oxidants. It moreover constitutes a barrier against the penetration of foreign substances and provides mechanic stability and tensile strength [1]. Various properties and components of the skin establish its barrier function. These include the outmost layer of the epidermis, the *stratum corneum* (SC), and the epidermis with its intercellular junctions that seal adjacent keratinocytes in the *stratum granulosum* (SG) [1,2]. The SC consists of completely keratinized, flattened, and dead corneocytes (terminally differentiated keratinocytes), which are surrounded by a protein-lipid-polymer structure, forming a water-repellent protective layer [3]. The cells of the lower epidermal layers are connected through cell-cell connections such as tight junctions (TJ), adherence junctions (AJ) at the apical side of the epithelial cells, and gap junctions (GJ). These junctions facilitate mechanical cohesion, communication, and the formation of an effective diffusion barrier [4]. TJ constitute the major physical barrier structure of the skin beside the SC and are composed of transmembrane proteins such as claudins, occludin, junctional adhesion molecules, and TJ plaque proteins [5]. Just beneath the TJ, epithelial cells are connected via AJ that are essential for mechanic stability. The adhesion molecules of AJ are transmembranal cadherins bound intracellularly to the actin cytoskeleton via catenin, vinculin, and α-actinin [6]. GJ are channels for intercellular cell-cell communication (GJIC), which allow the exchange of water, ions, and organic molecules between skin cells. They are an essential component of a functional epidermis and dermis [7]. GJ consist of connexons,

* Corresponding author.
E-mail address: sander.bekeschus@inp-greifswald.de (S. Bekeschus).
[1] contributed equally as second authors.

https://doi.org/10.1016/j.freeradbiomed.2020.09.026
Received 18 August 2020; Received in revised form 21 September 2020; Accepted 28 September 2020
Available online 01 October 2020

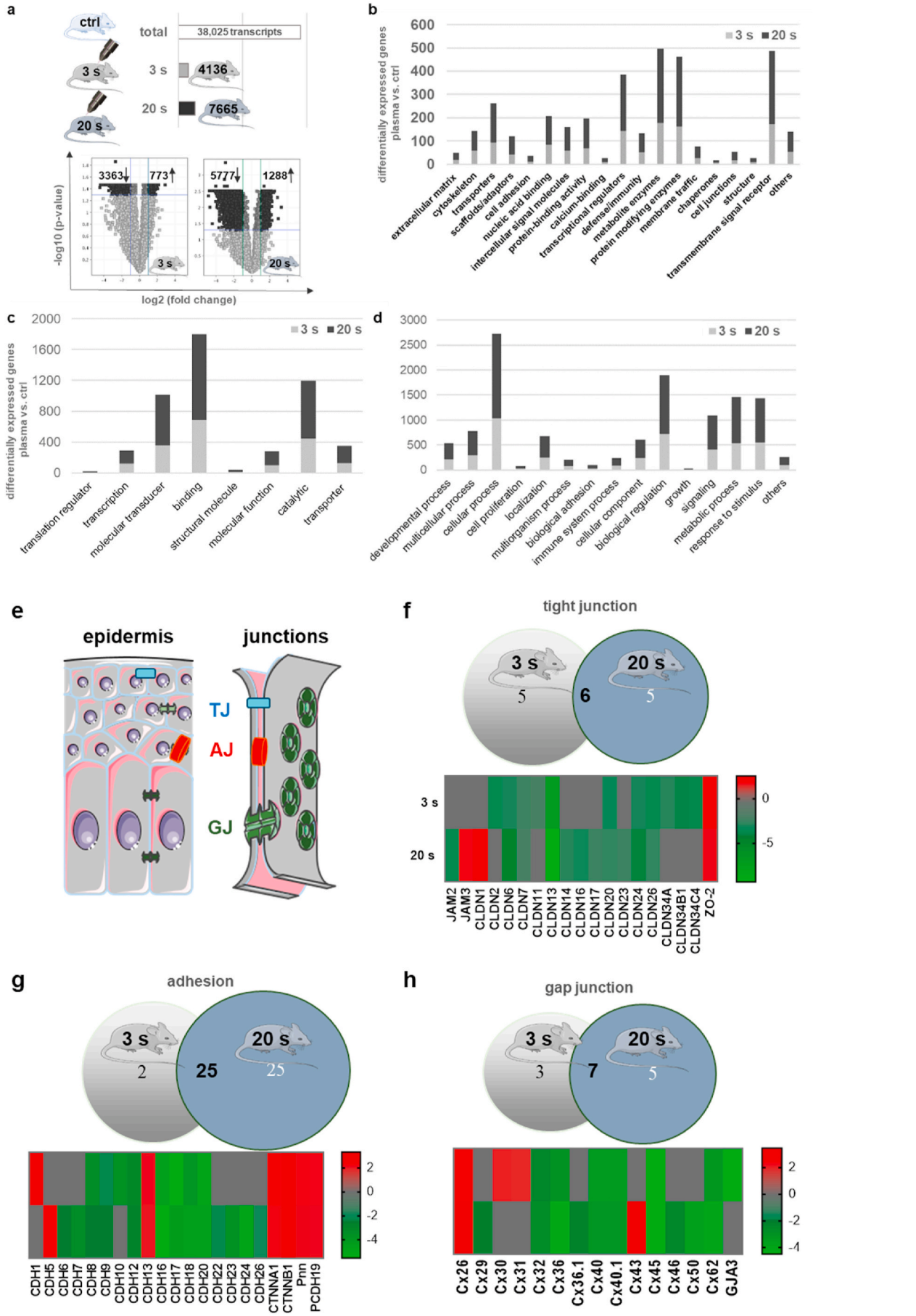

(caption on next page)

Fig. 1. The junctional network of the skin is differentially regulated after plasma treatment. (a) Flowchart and number of annotated differentially expressed genes identified by transcriptomic analysis in murine, intact skin exposed to either 3 s or 20 s of plasma treatment *in vivo*. A total of 38,025 transcripts were investigated (n = 9). Volcano plot displaying differentially expressed genes between plasma-treated and untreated control tissues. The vertical axis (y-axis) corresponds to the mean expression value of log 10 (p-value), and the horizontal axis (x-axis) displays the log 2 *fold change* value. The bold dots represent the upregulated genes (positive x-values) and down-regulated genes (negative x-values) with $p \leq 0.05$. (b–d) Classification of biological processes by gene ontology, and pathway information from the PANTHER database for protein classes (b), molecular functions (c), and biological processes (d). (e) Schematic of epidermal layers with tight junctions (TJ), adherence junctions (AJ), and gap junctions (GJ). (f–h) Venn diagrams showing the overlap of the transcripts and heat maps of the genes differentially expressed in plasma-treated compared to untreated control skin for TJ (f), adhesion (g), and GJ (h). The number of regulated genes and amplitude of regulation (green, down-regulated; red, upregulated) are indicated. JAM, junctional adhesion molecule; CLDN, claudin; ZO, zonula occludens protein, CDH, cadherin; CTNN, catenin; Pnn, pinin; PCDH, protocadherin; Cx, connexin; GJA, gap junctional protein. (For interpretation of the references to color in this figure legend, the reader is referred to the Web version of this article.)

which are composed of integral membrane proteins, i.e., connexins that are forming hexameric arrangements and channels between neighboring cells [8]. At the basal side, the epithelial cells are connected by desmosomes, which represent strong adhesion contacts and bear the main burden of intercellular adhesion in the epidermis [9]. Components of the extracellular matrix (ECM), such as collagens, are significant constituents of the dermis, form fibers, and facilitate skin elasticity and tear resistance. Furthermore, the dermis is not directly responsible for the skin barrier function but for balanced water content in the tissue and serves to supply the epidermis with nutrients [10].

However, the junctional network and barrier function of the skin is impaired in several types of disease. On the one hand, inflammatory skin disorders, e.g., psoriasis [11], atopic dermatitis [12], or actinic keratosis [13], are strongly associated with defective expression of TJ components. Moreover, the epidermal TJ network is dynamically regulated by the inflammatory milieu [12,14]. On the other hand, the physiological barrier function of the skin limits the penetration of topically-applied therapeutic substances under certain circumstances [15–17]. The cells in both the dermis and epidermis respond to reactive oxygen species (ROS) via redox signaling as a consequence of environmental stressors or local disturbances of tissue homeostasis [18,19]. Although ROS are often described as harmful agents, they have important roles in regulating physiological processes. ROS eliminate dysfunctional proteins by oxidation [20], increase tissue perfusion and oxygenation [21,22], and change the barrier permeability [23,24]. Hence, it seems plausible to capitalize on these evolutionary-conserved pathways for therapeutic purposes, such as modulating the skin barrier for enhanced oxygenation or drug uptake using a locally restricted deposition of bio-relevant amounts of ROS. Cold physical plasma is a partially ionized gas generating a diverse range of reactive particles. Besides charged particles (e.g., molecule ions, electrons), radiation (e.g. visible light; VIS, ultraviolet; UV, and near infrared radiation; IR), and electromagnetic fields, the most important biologically active components of plasmas are ROS (e.g., atomic oxygen, O; ozone, O_3; singlet delta oxygen, $^1O_2$; superoxide, $O_2^{\bullet-}$; hydrogen peroxide, H_2O_2; hydroxyl radical, •OH; nitric oxide, •NO; nitrogen dioxide radical, $\bullet NO_2$; peroxynitrite, $ONOO^-$) [25,26]. Moreover, the question is whether therapeutic plasma treatment is, in principle, capable of modulating the junctional network, which might be important to tackle inflammatory skin diseases.

To this end, we investigated the molecular and functional consequences of therapeutic ROS in the intact skin of SKH1 mice *in vivo*. Exogenous and local ROS generation was facilitated using cold plasma technology, a medically accredited tool to perform such tasks [27]. Utilizing transcriptomic and lipidomics technology together with a molecular analysis of the junctional network, we identified how topically applied plasma-generated ROS alters the penetration of the lipophilic model drug curcumin and promotes the perfusion and oxygenation of skin tissue *in vivo*.

2. Results

2.1. Plasma treatment of murine skin elicited profound changes in gene expression profiles

To analyze the entire transcriptome of the skin tissue, global expression analysis was performed 24 h after plasma treatment (3 s or 20 s per mm^2) and compared to gene expression in untreated control skin. 38,025 different transcripts were analyzed to identify genes in the plasma-treated samples that significantly ($p \leq 0.05$) changed their expression more than ± 2-fold compared to controls. For tissue samples of plasma-treated animals from a remote skin area that had not received plasma exposure (0 s), no significantly different gene expression was found compared to the untreated control mice (data not shown). For a treatment duration of 3 s and 20 s, 4136 and 7665 annotated genes were identified, respectively. Volcano plot displaying differentially expressed genes between plasma-treated and untreated samples showed 773 and 1288 upregulated as well as 3363 and 5777 down-regulated genes after 3 s and 20 s, respectively (Fig. 1a).

To determine the biological relevance of the differentially expressed genes identified in plasma-treated skin, a functional gene ontology (GO) analysis was performed using the PANTHER classification system. The patterns of gene regulation were similar between 3 s and 20 s of treatment, as seen by the assignment to similar molecular functions (Fig. 1b), protein classes (Fig. 1c), and biological processes (Fig. 1d). The annotated genes were assigned to 22 different protein classes. Among the main categories comprising the most regulated genes, we identified several classes such as *gene-specific transcriptional regulators*, *metabolite enzymes*, *protein modifying enzymes,* and *transmembrane signal receptors*. About 1% of the analyzed genes were assigned to the protein class *cell adhesion* and *junctions* (Fig. 1b). Gene regulation within the category of molecular functions was dominant for *binding*, *catalytic activity*, and *signal transduction* (Fig. 1c). In addition, in the category biological processes, the identified genes were assigned to 22 different processes (with a selection of 14 being shown in Fig. 1d), including *cellular and metabolic processes*, *biological regulation*, *signaling*, and *responses to stimulus*, which accounted for the largest share of these.

For maintenance of the skin barrier function, several classes were found, including genes related to cell junctions, especially tight junctions (TJ), adherence junctions (AJ), and gap junctions (GJ) (Table 1). Integral proteins of TJ were mainly down-regulated with some exception for claudin 1 (*CLDN1*) and the junctional adhesion molecule 3 (*JAM3*), as well as zonula occludens 2 (*ZO-2*), which were upregulated in response to plasma treatment (Fig. 1e). Genes assigned to the process of biological adhesion and the protein class of cell adhesion molecules are important for the interconnection of cells and the adhesion to the ECM [28]. These include protocadherins, cadherins, desmosomes, and hemidesmosomes that were either up or down-regulated after plasma treatment. The cadherin signaling-associated catenins (*CTNNB1, CTNNA1*), a transcriptional activator of E-cadherin pinin (*PNN*), and

Table 1
Differentially expressed transcripts of cell junctions and adhesions. n.s. = non-significant.

Gene symbol	Gene name	Fold change 3 s	20 s	Function
Tight junction (TJ)				
CLDN1	claudin 1	n.s.	+2.52	integral membrane protein, interacting with Cldn3 and 5
CLDN2	claudin 2	-3.01	-3.64	membrane protein, form paracellular water channels
CLDN6	claudin 6	-3.14	-4.73	epithelialization, differentiation
CLDN7	claudin 7	-2.56	-2.19	epithelial TJ protein
CLDN13	claudin 13	-7.19	-9.34	membrane protein, erythropoiesis
CLDN20	claudin 20	-3.39	-2.82	membrane protein
CLDN24	claudin 24	-3.14	-4.19	membrane protein
CLDN26	claudin 26	-3.76	-2.81	membrane protein
JAM2	junctional adhesion molecule 2	-2.94	-3.71	endothelial TJ protein, transmigration of leukocytes
JAM3	junctional adhesion molecule 3	n.s.	+1.65	endothelial, epithelial TJ protein, in fibroblasts expressed
Adherence junction (AJ)				
CDH1	cadherin 1	+2.60	n.s.	epithelial cadherin, cell adhesion
CDH8	cadherin 8	-3.47	-2.54	integral membrane, calcium-dependent cell-cell adhesion
CDH13	cadherin 13	+2.06	+2.01	GPI-anchored T-cadherin, cell migration, stress fiber formation
CTNNA1	α-catenin	+2.33	+2.21	binds to cadherins, linked to actin cytoskeleton
CTNNB1	β-catenin	+3.32	+3.33	binds to cadherins, linked to actin cytoskeleton
PCDH1	protocadherin 1	-3.71	-3.04	calcium-dependent cell adhesion molecule
PCDH10	protocadherin 10	-3.25	-4.13	calcium-dependent cell adhesion molecule
PCDH15	protocadherin 15	-2.92	-3.13	calcium-dependent cell adhesion molecule
PCDH17	protocadherin 17	-4.68	-4.67	calcium-dependent cell adhesion molecule
PCDH19	protocadherin 19	+2.15	+2.05	calcium-dependent cell adhesion molecule
PNN	pinin	+2.15	+2.12	transcriptional activator of E-cadherin
Desmosomes				
DSP	desmoplakin	+2.12	+1.75	main component of desmosomes
DSG2	desmoglein 2	-3.71	-2.65	intracellular component of desmosomes
DSG4	desmoglein 4	-3.59	-3.94	intracellular component of desmosomes
Gap junction (GJ)				
Cx26 (GJB2)	GJ protein β2	+2.40	+2.52	structural component of GJ, tumor suppression, migration, invasion
CX30 (GJB6)	GJ protein β2	+2.03	n.s.	structural component of GJ
CX31 (GJB3)	GJ protein β3	+1.93	n.s.	structural component of GJ
CX32 (GJB1)	GJ protein β1	-2.44	-2.71	structural component of GJ
Cx33 (GJA6)	GJ protein α6	-4.49	-4.40	structural component of GJ
Cx36 (GJD2)	GJ protein 2	-3.04	-4.35	structural component of GJ
Cx39 (GJD4)	GJ protein δ4	-3.42	-3.15	structural component of GJ, multi-pass membrane protein
Cx45 (GJC1)	GJ protein χ1	n.s.	+2.59	structural component of GJ, binding to ZO-1
Cx43 (GJA1)	GJ protein α1	n.s.	+3.46	structural component of GJ, GJIC, inflammation, wound healing

genes assigned to the integrin signaling were found to be upregulated (Fig. 1f). Structural components of GJ are connexins, which were either upregulated (e.g., Cx26/30/31/43) or down-regulated (e.g., Cx32/36/40/45/62) in response to plasma (Fig. 1g).

Among the genes related to the maintenance of cellular shape, stabilizing the cell structure, and anchoring of proteins for cell adhesion molecules, we identified cytoskeletal proteins (Table 2). Some components of the cytoskeleton or proteins that are important for dealing with mechanical stress were found to be upregulated (*CLAPS1, EPPK1*), while others were down-regulated after plasma treatment (*ACT7A, TUBA3A*). Different subgroups of keratins representing an essential intermediary filament in keratinocytes were also differentially regulated. One of the most important and frequently occurring proteins in the ECM is collagen. There are many different types of collagen, and these have been upregulated (*COL1/4/6/18*) or down-regulated (*COL9/19/11/12/24/25*) after plasma treatment (Table 2). A complete table of all differentially expressed genes is given in the Omnibus database (GSE152933).

2.2. Plasma treatment of murine skin affected the junctional network and ECM

Transcripts of selected target genes playing a role in maintaining barrier function were validated using qPCR. These included transcripts coding for proteins of cell-cell connections in TJ, AJ, and GJ, and components of the ECM. Claudin 1 (*CLDN1*) expression doubled in response to plasma treatment. Zonula occludens 1 (*ZO-1*), responsible for binding integral membrane proteins and anchoring them to the actin cytoskeleton, was down-regulated in the skin of plasma-treated animals. In addition, β-catenin 1 (*CTNNB1, upregulated*) and vinculin (*VCL, unchanged*) are molecules that bind intracellularly to the adhesion molecules and create a stabilizing connection to the actin cytoskeleton (Fig. 2a). For the GJ components, *Cx26* was found to be down-regulated, while a marked and modest upregulation was found following plasma treatment for *Cx31* and *Cx43*, respectively. Pannexins are structurally similar to connexins and form membrane channels that allow the exchange and transport of substances between the intracellular space and the ECM. Only a tendency of increased *PANX1* expression was found after plasma treatment (Fig. 2b). The ECM comprises many different proteins, two important ones being collagen 1A1 (COL1A1) and fibronectin (FN1). *COL1A1* expression was approximately three-fold higher in 3 s and two-fold higher in 20 s plasma-treated tissue. Differential expression of *FN1* was 5.8-fold increased after 3 s plasma treatment, while after 20 s plasma treatment, an increase by a factor of 11.2 was found compared to the untreated control. The gene expression of keratin 1 (*KRT1*), which is found in keratinized structures of the epidermis, was unchanged for plasma treatment, while Keratin 14 was found to be dramatically enhanced. (Fig. 2c). Cytokines not only regulate the growth and differentiation of cells but also are essential for the formation of the lipid mantle around the cells in the *stratum corneum* (SC) by stimulation of lipid synthesis, making them indispensable for skin integrity. Interleukin 6 (*IL6*) expression was stimulated by exposure to cold plasma. For 3 s treatment, a doubling, and for 20 s, a 2.5-fold increase of gene expression was determined compared to the control. The expression of tumor necrosis factor α (*TNFα*) was slightly increased for a 3 s and decreased below the control level (0.7 fold-change) after 20 s of plasma treatment (Fig. S1).

The next question was whether plasma treatment significantly

Table 2
Differentially expressed transcripts of cytoskeletal and matrix proteins. n.s. = non-significant.

Gene symbol	Gene name	Fold change		Function
		3 s	20 s	
Mechanics and cytoskeleton				
CLASP1	CLIP-associated protein 1	+2.11	+2.15	binding on + -terminus of microtubules and their stabilization
EPKK1	epiplakin 1	+2.07	+2.07	cytoskeletal linker protein, binds to intermediate filaments, controls their reorganization after stress response
KRT12	keratin 12	-3.38	-4.15	intermediate filament, structural component of cytoskeleton
KR15	keratin 15	+2.68	+2.02	intermediate filament, structural component of cytoskeleton
KRT25	keratin 25	+2.52	+3.65	intermediate filament, structural component of cytoskeleton
KRT28	keratin 28	n.s.	+2.73	intermediate filament, structural component of cytoskeleton
KRT35	keratin 35	+2.83	+2.13	intermediate filament, structural component of cytoskeleton
KRT42	keratin 42	-3.18	-4.57	intermediate filament, structural component of cytoskeleton
KRT22	keratin 222	-4.20	-5.59	intermediate filament, structural component of cytoskeleton
ACTL7a	actin-like 7a	-2.86	-2.47	structural component of cytoskeleton
ACTL7b	actin-like 7b	-2.85	-3.73	structural component of cytoskeleton
ACTL11	actin-like 11	-4.61	-3.27	structural component of cytoskeleton
TUBA3A	α tubulin 3A	-2.83	-4.22	main component of microtubules
Extracellular matrix				
COL1A1	collagen type I, α1	n.s.	+1.83	component of ECM, angiogenesis
COL4A1	collagen type IV, α1	+3.10	+4.42	component of ECM, angiogenesis
COL4A2	collagen type IV, α2	+2.06	+2.54	component of ECM, angiogenesis
COL6A1	collagen type VI, α1	n.s.	+2.26	major structural component of microfibrils
COL6A3	collagen type VI, α3	+3.11	+4.87	aids in microfibril formation, binds ECM proteins, DM
COL9A1	collagen type IX, α1	-3.28	-3.77	component of ECM, flexible nature
COL10A1	collagen type X, α1	n.s.	-2.09	component of ECM, biomarker of wound healing
COL11A2	collagen type XI, α2	-2.81	-3.24	minor fibrillar collagen
COL12A1	collagen type XII, α1	-3.22	-3.37	component of ECM
COL18A1	collagen type 18, α1	+2.62	+2.60	multiplexin extracellular matrix protein
COL24A1	collagen type 24, α1	-2.80	-2.66	component of ECM
COL25A1	collagen type 25 α1	-3.77	-3.09	component of ECM
FBN1	fibulin 1	+2.17	+2.06	part of ECM fibrils, cell adhesion and migration
FBN1	fibrillin 1	+2.87	+2.90	structural component of microfibrils of ECM
HAPLN4	hyaluron and proteoglycan-linked protein 4	-3.06	-3.48	formation of ECM by binding on hyaluronic acid

affected the protein expression levels of several junctional targets (Fig. 2d). Following the expression data, the protein amount of claudin 1 increased after plasma treatment. With the 3 s and 20 s plasma exposure time, the protein expression was three- and four-fold increased compared to untreated control samples, respectively. Surprisingly, the occludin expression remained unchanged regardless of the plasma treatment time. β-catenin was increased approximately two-fold following 3 s and 20 s of plasma exposure. The plasma treatment also induced a three-fold higher expression of E-cadherin (3 s). The expression of connexin 31 did not differ significantly between samples (fold-change of 1.8 for 20 s). Corresponding to the results retrieved in gene expression analysis, the protein amount of connexin 43 was 3.5 times higher than in untreated control skin. For the intermediary filament keratins 1 and 14, the changes were also consistent with the gene expression data. Keratin 1 protein expression was unchanged. The significant increase in keratin 14 expression was 4.2 and 5.2 for 3 s and 20 s, respectively.

This spurred the question of whether up or down-regulation of TJ proteins observed after plasma treatment might relate to their localization or distribution. For this, claudin 1 (Cldn1) immunofluorescence was visualized in the epidermis from the basal layers up to *stratum granulosum* (SG), and the epithelial cell layer around the sebaceous glands (Fig. 2eI). Occludin (Ocln) showed the characteristic fence-like geometry in the upper epidermal layers (Fig. 2eII). Zonula occludens 1 (ZO-1) was detected in the epidermal and dermal cell layers (Fig. 2eIII). Connexin 31 (Cx31) was expressed strongly in the outmost epithelial cells of the SG (Fig. 2eIV). Connexin 43 (Cx43) was localized in all layers of the epidermis and showed characteristic focal localization, which might be communication channels (connexons) between the cells (Fig. 2eV). Keratin 1 (Krt1) was confirmed in the upper skin layers, especially in the SG (Fig. 2eVI). It can be easily distinguished from Krt14; this intermediate filament is found mainly in the basal layers of the epidermis (Fig. 2eVII). Higher image magnifications of the localization of these proteins are shown in the bottom lane (Fig. 2e). Plasma treatment of the skin did not induce alterations of the spatial distribution of Cldn1, Ocln, ZO-1, Cx31/43, and Krt1/14. Using immunofluorescence microscopy, neither a translocation into other cell areas or tissue layers was detected, nor structural features were affected. However, we found a similar expression pattern of the selected targets (Fig. 2f), confirming our quantification analyses using qPCR and Western blot.

To analyze putative mechanisms related to the effects observed, we determined the junctional protein expression and changes in their distribution at a single-cell level *in vitro* in primary keratinocytes forming epidermal layers (Fig. 3a). First, gap junction intercellular communication (GJIC) was assessed using the scrape loading dye transfer (SLDT) assay to determine the functional activity of the GJ. The lucifer yellow (LY) represented the dye being transferred through functional GJ-communicating keratinocytes, and the texas red-dextran (TR-Dx) labeled GJ-impermeable cells (Fig. 3b). 15 min, 1 h, and 24 h after plasma treatment, we obtained an increased uptake of LY in a high number of cells being apart at larger distances from the initial scrape when compared to control samples, suggesting a plasma-driven improvement of GJIC (Fig. 3c). Next, intracellular Cx43 was analyzed using immunofluorescence staining to elucidate the mechanisms underlying an increased GJIC after plasma treatment. Specific Cx43-positive spots were detected in the membrane (arrowhead), indicating GJ plaques and well-defined bundles of the actin cytoskeleton (Fig. 3dI). In line with the qPCR and Western blot results, we identified a noticeable increase of Cx43 at the cell borders at 6 h (Fig. 3dII) and 24 h (Fig. 3dIII) after plasma treatment. The data suggested that plasma treatment strengthened the GJIC due to the activation of signaling events *in vivo*. Contrary to the *in vivo* results, we found a noticeable but transient increase of occludin 1 h after plasma exposure (Fig. 3eII),

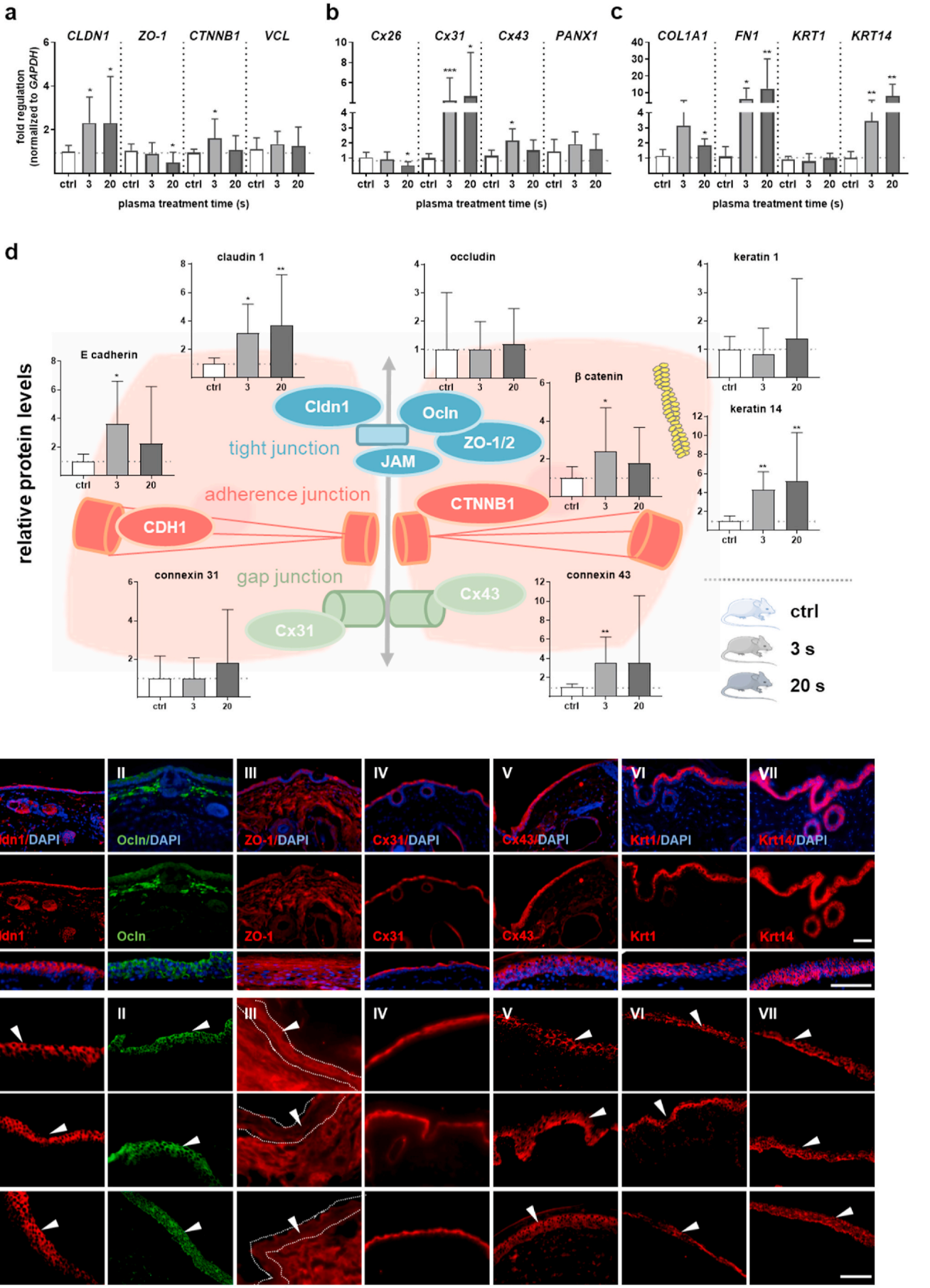

(caption on next page)

Fig. 2. Transcriptomic analysis-derived target confirmation in plasma-treated skin tissue. (a–c) qPCR-based gene expression analysis of selected targets of (a) tight junctions (e.g., *CLDN1* and *ZO-1*) and adherence junctions (*CTNNB1* and *VCL*), (b) gap junctions (e.g., *Cx26/31/43* and *PANX1*), and (c) extracellular matrix (ECM) components (e.g., *COL1A1* and *FN1*) and epidermal proteins (e.g., *KRT1/14*). (d) Western blot analysis (WB) of selected junctional targets (e.g., claudin 1, occludin, β-catenin, E-cadherin, connexins 31/43, keratins 1/14). (e) Overview of immunolocalization of Cldn1 (I), Ocln (II), ZO-1 (III), Cx31 (IV), Cx43 (V), Krt1 (VI), and Krt14 (VII) with or without nuclear counterstaining (DAPI, blue, upper two lanes), and representative images of the spatial distribution of selected targets (bottom panel) in higher magnification in murine, intact, untreated skin. (f) Higher image magnification of the corresponding immunofluorescence stainings in skin being either left untreated (upper images) or 24 h post-exposure to 3 s (middle images) and 20 s (bottom images) of plasma treatment as visualized by immunofluorescence microscopy. Results are expressed as mean + SEM of at least 4 experiments with several replicates ($n \geq 4$). Statistical analysis was performed using one-way analysis of variances against the control condition with $p < 0.05$ (*), $p < 0.01$ (**), and $p < 0.001$(***), and normalization to GAPDH (a). Scale bars are 50 μm. (For interpretation of the references to color in this figure legend, the reader is referred to the Web version of this article.)

whereas ZO-1 was found to be down-regulated 24 h after plasma exposure (Fig. 3eIII) when compared to controls (Fig. 3eI), again validating the qPCR results obtained above. The distribution of adhesion proteins such as E-cadherin and β-catenin, however, remained unchanged in keratinocytes (Fig. S2).

2.3. Plasma treatment increased oxygenation and hemoglobin index in the skin

Since plasma treatment generates a plethora of ROS simultaneously, which directly act on the skin and are known to induce redox signaling processes, it was natural to investigate physiological parameters of this organ following plasma treatment *in vivo*. Using the hyperspectral camera system and analysis software TIVITA, microcirculatory parameters in the skin were analyzed before, 10 min (corresponding to 0.17 h), 6 h, and 24 h after plasma treatment in mice (Fig. 4). After plasma treatment, the changes were already visible in the camera images of the TIVITA system for 3 s (Fig. 4a–d) and 20 s (Fig. S3). The relative oxygen saturation (StO_2) of the blood of superficial tissue layers is indicated by the oxygenation. Ten minutes and 24 h after the plasma treatment, StO_2 was significantly higher than before the treatment for the skin areas exposed to plasma (both for 3 s and 20 s conditions). After 6 h, no changes in oxygenation were observed (Fig. 4a'). From the analyzed spectral data, the peak around 550–570 nm was altered after plasma treatment from one to a double peak validating the noticeable plasma-induced oxygenation in superficial skin layers (Fig. 4a''). The

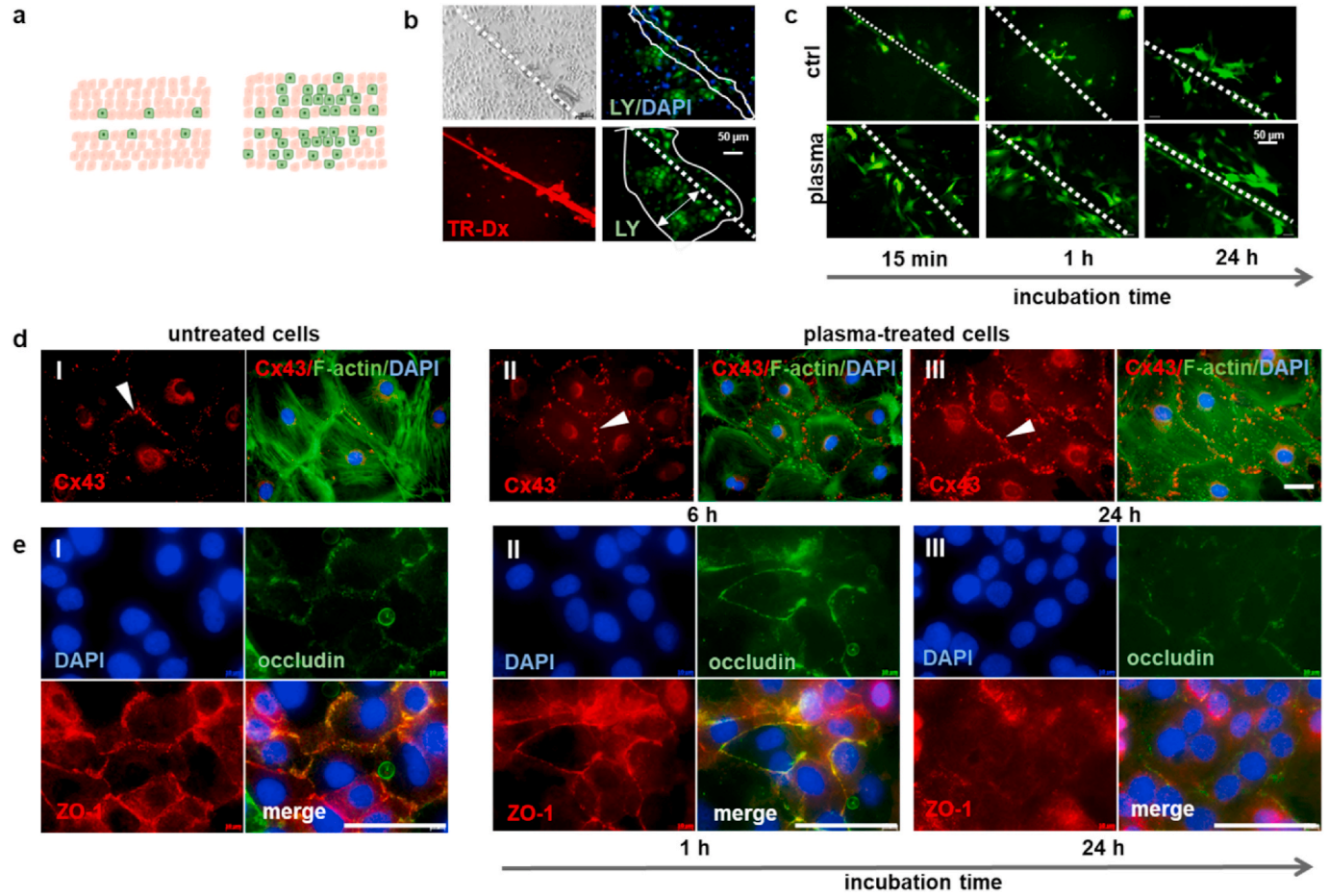

Fig. 3. Plasma accelerated functional GJIC and changed the expression of TJ proteins. (a) Schema of scrape-loading dye transfer (SLDT) assay in skin cells. (b) Epidermal keratinocytes were isolated from untreated murine skin and a SLDT assay using GJ-permeable lucifer yellow (LY, green) and GJ-impermeable texas red-dextran (TR-Dx) was performed (scrape, dotted line; asterisks, the distance of intracellular LY distribution). (c) SLDT was done after 15 min, 1 h, and 24 h post-treatment in keratinocytes ($n \geq 4$). (d) Immunofluorescence microscopy of Cx43 (red) and F-actin using FITC-phalloidin (green) at 6 h (II) and 24 h after plasma treatment (III) in comparison to untreated cells (I). (e) Co-staining of occludin (green) and ZO-1 (red) at 1 h (II) and 24 h post-exposure to plasma (III) in comparison to untreated cells (I). Nuclei were counterstained with DAPI (blue). Scale bars are 50 μM (b–d), and 10 μM (e). (For interpretation of the references to color in this figure legend, the reader is referred to the Web version of this article.)

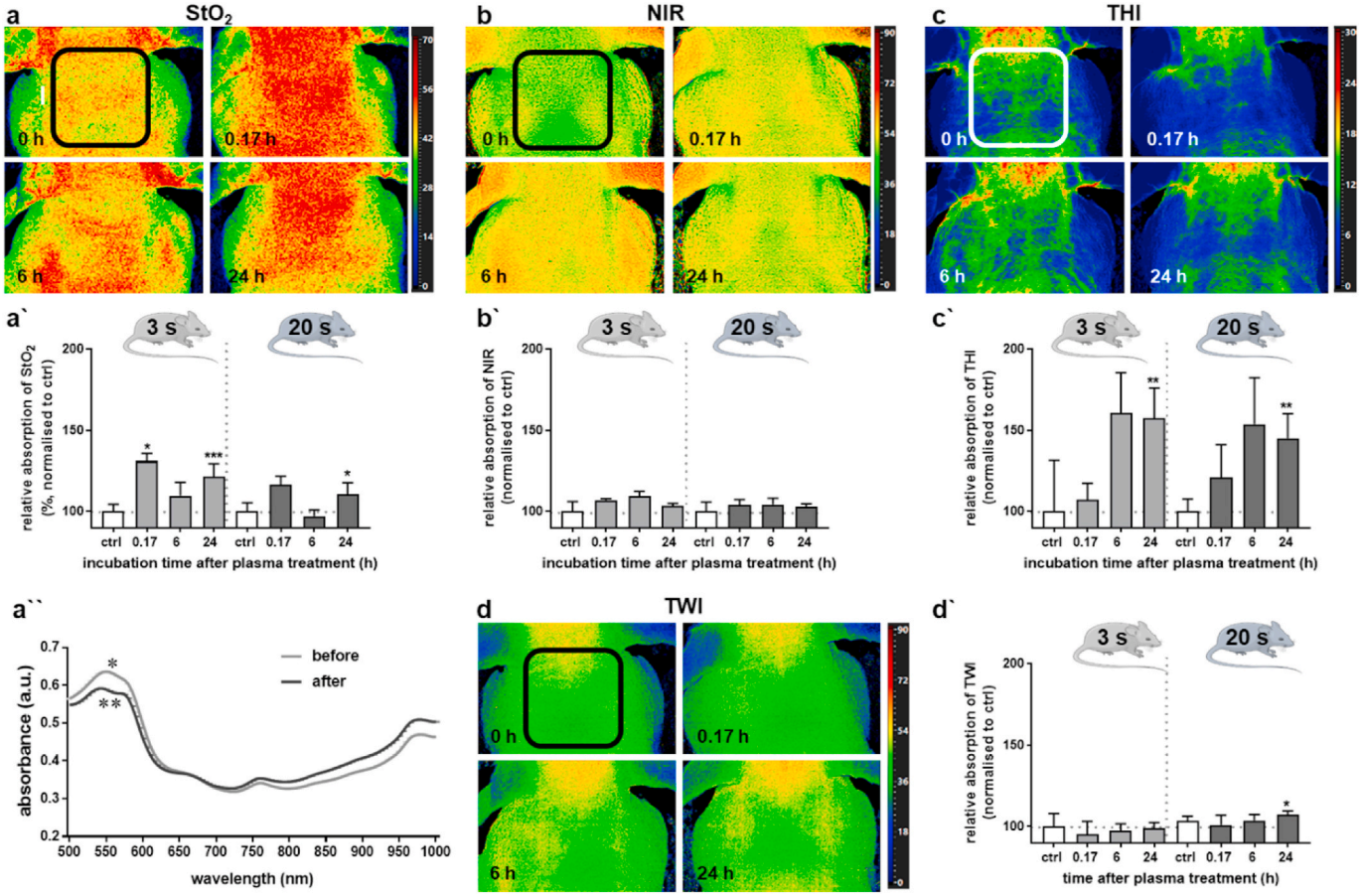

Fig. 4. Plasma treatment modulated microcirculatory parameters of murine skin *in vivo*. (a–d) Representatives false-colored images of murine skin exposed to plasma for 3 s before treatment 0 h, and after 0.17 h, 6 h and 24 h (quadrat = area of treatment). (a'-d') Quantification of hyperspectral imaging parameters in the skin of mice exposed to 3 s (left part of the diagrams) or 20 s (right part of the diagrams) of plasma treatment, including tissue oxygenation (StO_2, a) and perfusion in deeper layers (NIR, b) as well as the tissue hemoglobin index (THI, c) and tissue water index (TWI, d). (a") High-resolution HSI analysis in the range of 500–1000 nm allowed for calculating four parameters before after plasma treatment. The tissue oxygenation was increased upon plasma treatment resulting in changes from one (*) to double peak (**) at 550–570 nm. Results are expressed as mean + SEM of at last four independent measurements, and statistical analysis was performed using unpaired *t*-test with **, $p < 0.01$ and ***, $p < 0.001$ (n = 4).

oxygen saturation of the blood in deeper tissue layers was determined with the near-infrared perfusion index (NIR), showing no changes of perfusion in deeper skin layers (Fig. 4b'). Likewise to oxygenation, the tissue hemoglobin index (THI) was slightly (after 10 min and 6 h) and significantly (after 24 h) higher than before the treatment for the skin areas exposed to plasma (both for 3 s and 20 s conditions, Fig. 4c'). The tissue water index (TWI) was slightly lower for 3 s than before the treatment and increased significantly 24 h after treatment for 20 s conditions (Fig. 4d'). Altogether, our data confirmed plasma treatment to modulate the tissue oxygenation and hemoglobin indices in superficial skin layers.

2.4. Analysis of lipids of the skin following plasma treatment in vivo revealed oxidative modifications and changes in the relative abundance of lipid classes

Plasma treatment affected the junctional network, tissue oxygenation, and perfusion. As plasma-derived ROS reach the skin from the apical side, we hypothesized to find changes in the lipid composition or their modifications within the skin, which would decrease with increasing tissue depth. For this, tape stripping on the skin was performed after plasma treatment (3 s/mm^2) to determine the SC lipid profile in combination with LC/MS^2. To avoid analyzing any alterations that might be due to putative environmental contaminants, the outermost layer was discarded (Fig. 5a), and the 9 subsequently sampled tape strips were collected. H&E staining of tissue demonstrated the complete removal of SC after plasma treatment (Fig. 5b). By LC/MS^2, ten lipid classes of the sebaceous gland and epidermal origin were identified (Fig. 5c). The most abundant lipid classes were ceramides and triglycerides and their putative oxidative modifications, which covered up to over 90% of the identified SC lipids. The abundance profile differed significantly after plasma treatment. Triglycerides as part of sebaceous lipids were less abundant after treatment (up to 10% decreased). Other lipid classes such as cholesterylester and diacylglycerides were also decreased after treatment. Other lipid classes were identified in low abundances with no significant changes. In parallel to alterations of the lipid class composition, the number of individual lipid species changed with the location in the SC. In deeper layers, a decreasing number of lipid species (layer 2,3,4: 175 species; layer 5,6,7: 165 species; layer 8,9,10: 152 species) was identified (Fig. 5d). Additionally, in this class, 34 lipid peroxidation products (LPP) in control and after plasma treatment were found (Table 3). Among epidermal lipids, ceramides were identified in high numbers with increasing abundance upon plasma treatment. In this class, two subclasses (di- and trihydroxy ceramides) were identified. Both dihydroxy ceramide subclasses, specifically amide-linked non-hydroxy and α-hydroxy fatty acid ceramides, increased in all layers upon plasma treatment (Fig. 5e).

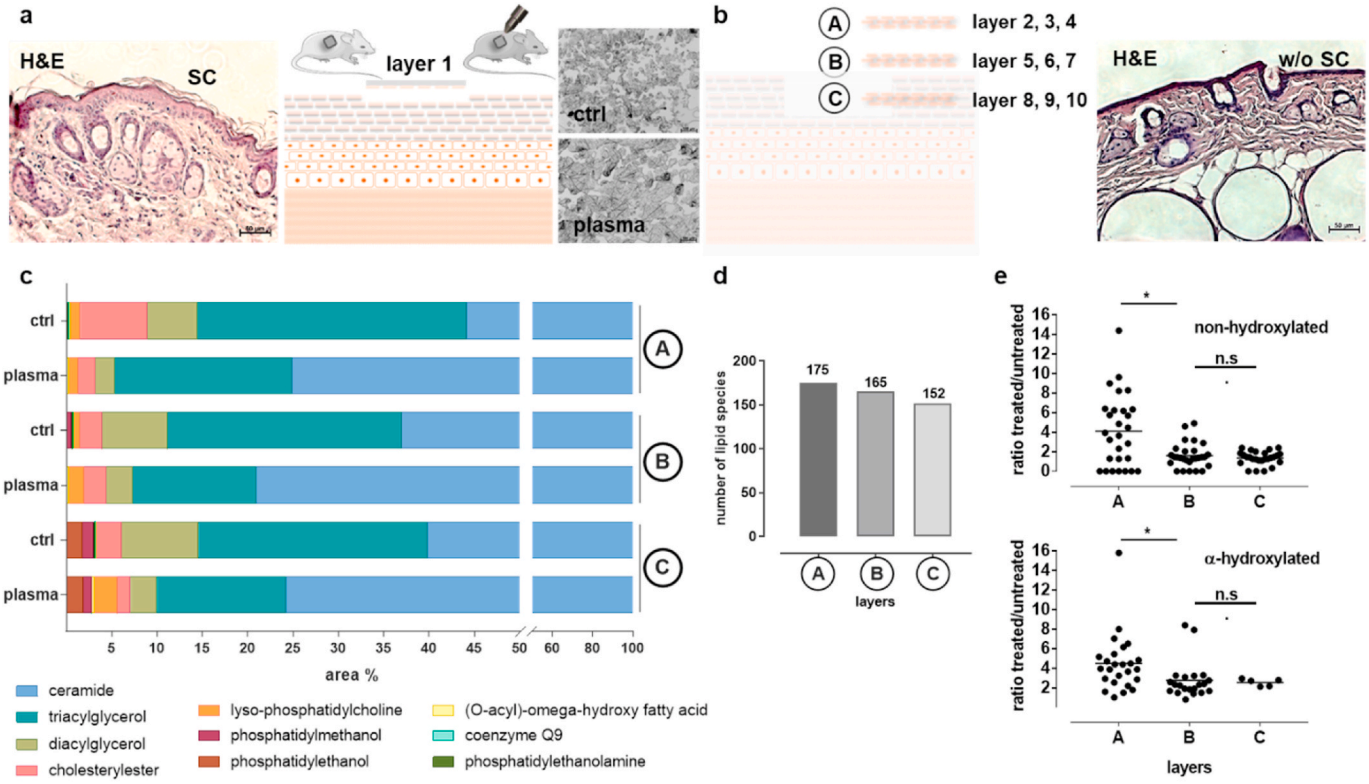

Fig. 5. Lipids identified in individual layers of the *stratum corneum* (SC) of murine skin. (a) H&E staining of murine skin with intact *stratum corneum* (SC), schematic of the tape stripping process, and representative brightfield image of corneocytes on the tape after stripping off the first corneocyte layer. (b) Tape stripping of SC-layers 2–10 of the skin of untreated and plasma-treated animals (3 s/mm^2), and representative H&E staining of murine skin with 10 layers of the SC being stripped off. Three adjacent layers were summarized into one sample and labeled with A for layers 2–4, B for layers 5–7, and C for layers 8–10. (c) Relative abundance of SC-derived lipids and putative oxidative modifications of individual SC-layers analyzed using LC/MS^2 (area of peak in %). (d) Number of lipid species in layers A (175), B (165), C (152). (e) Non-hydroxylated and α-hydroxylated dihydroxyceramide fatty acids across the different SC-layers shown as a ratio of plasma-treated over untreated skin for different SC layer composites. Results are from several technical replicates of 4 animals per group. Statistical analysis was performed using unpaired ANOVA/Tukey's test with $p < 0.05$ (*); n.s. = not significant (n = 3).

2.5. Plasma treatment increased skin SC disaggregation and curcumin penetration in vivo

Changes in the junctional network and lipid composition might have affected the skin barrier function. To investigate this hypothesis, we tested whether plasma treatment led to changes in this barrier histologically and via analysis of curcumin penetration into the skin. Curcumin is a lipophilic, natural, and fluorescent (550 nm) model drug derived from turmeric (curcuma). Histological analysis of the SC (using H&E staining) showed a modest but visible disintegration of the SC in plasma-treated skin tissues (arrows, Fig. 6a). Curcumin (green) penetration was tested by algorithm-driven image quantification after plasma treatment (3 s/mm^2, Fig. 6b). The thickness of the SC was determined in the tissue sections showing modest differences between the tissue samples of untreated (5.5 μm) and plasma-treated (6.1 μm) skin (Fig. 6c), underlining the findings in the H&E stained skin sections. Within the SC, significantly increased levels of curcumin were identified in skin exposed to plasma when compared to untreated control skin (Fig. 6d). In contrast to the SC, the fluorescence intensity (as a surrogate of curcumin penetration) in the epidermal region was similar in plasma-treated and control groups (Fig. 6e). These results indicated that the plasma treatment led to a decrease of the cell-cell contacts of the outer skin layers without affecting the penetrability of a lipophilic model drug into deeper epidermal and dermal layers.

3. Discussion

Cold plasma generates a plethora of different types of reactive species (ROS) [26,29,30], which can activate critical cellular signal transduction processes [31,32]. Consequently, redox signaling is involved in many cellular processes and is often described as the basis of the plasma effects [27,32–36]. However, the molecular and functional consequences of plasma treatment on the skin and its barrier function remain elusive. This is important because excessive oxidative stress causes malfunctions in skin homeostasis [37]. Thus, we used various biochemical, molecular, and modern imaging approaches to investigate plasma-induced changes in the skin in terms of barrier function and skin physiology. Our findings may also have therapeutic implications because the junctional network is dysregulated in several skin diseases (e.g., dermatitis, skin infection, lichen planus, psoriasis) [2,38].

Global gene expression in tissue depends on many factors, including cell type, developmental stage, and environmental stimuli, and can be regulated in various ways, including the redox level [39,40]. There are many genes whose expression is regulated by oxidation through, for instance, superoxide ($O_2^{\cdot-}$), hydrogen peroxide (H_2O_2), singlet oxygen ($^1O_2$), various reactive nitrogen oxides, and redox-active quinones [41]. These species are generated by cold plasma systems simultaneously [26]. In a plethora of studies, several techniques were applied to reveal possible reactions in the gas phase of plasmas [32,42–45]. This included modeling studies [46] together with the quantification of OH radical [47], peroxynitrite [48], ozone, and singlet delta oxygen [49] production. While technical tools are lacking to precisely disentangle their contribution to the biomedical effects observed in target tissues, the trajectories and anticipated concentrations of different types of ROS likely to interact with the target were investigated at great detail for the gas phase of kINPen [29]. For the *in vitro* part, indirect plasma

Table 3
Identified triglyceride oxidation products in control and after plasma treatment. Oxidation products were detected as [M + NH4] products in LipidSearch (c = ctrl; p = plasma).

Lipid peroxidation products (LPP)	Formula neutral	Monoisotopic mass	Layer A		Layer B		Layer C	
Oxygen addition products (OAP)			c	p	c	p	c	p
TG(18:1+2O_18:2_18:3)	C57H102O8N1	928.7605					x	
TG(18:1 + O_16:0_18:1)	C55 H106 O7 N1	892.7969					x	
TG(18:1 + O_17:0_20:0)	C58H114O7N1	936.8595		x				
TG(18:1 + O_17:0_20:1)	C58H112O7N1	934.8439		x				
TG(18:1 + O_18:0_18:1)	C57 H110 O7 N1	920.8282	x					
TG(18:1 + O_18:1_18:1)	C57 H108 O7 N1	962.8752	x		x		x	
TG(18:1 + O_18:1_18:2)	C57H106O7N1	918.8126	x				x	
TG(18:1 + O_19:0_20:1)	C60H116O7N1	962.8752		x				
TG(18:1 + O_20:0_20:0)	C61H120O7N1	978.9065		x				
TG(18:2+3O_16:0_18:1)	C55 H104 O9 N1	922.7711					x	
TG(18:2+3O_18:0_18:1)	C57H108O9N1	951.4712					x	
TG(18:2 + O_18:1_18:1)	C57H106O7N1	916.7969			x			
TG(18:2 + OO_16:0_16:0)	C53H102O8N1	880.7605	x					
TG(18:2 + OO_16:0_18:0)	C55H106O8N1	908.7918	x					
TG(18:2 + OO_16:0_18:1)	C55 H104 O8 N1	906.7762					x	
TG(18:2 + OO_18:1_18:1)	C57H106O8N1	932.7918	x	x	x	x	x	x
TG(18:2 + OO_18:1_18:2)	C57H104O8N1	930.7762	x		x		x	
TG(18:2 + OO_18:2_18:2)	C57H102O8N1	928.7605	x					
TG(18:2 + OO_20:0_20:0)	C61H118O8N1	992.8857		x		x		
TG(18:3 + OO_16:0_18:1)	C55 H102 O8 N1	904.7605					x	
TG(18:3 + OO_18:1_18:1)	C57 H104 O8 N1	930.7762	x			x	x	
Oxygen cleavage products (OCP)								
TG(5:0COOCH3_16:0_16:0)	C41H80O8N1	714.5884			x		x	
TG(9:0CHO_15:0_15:0)	C42H82O7N1	712.6091	x	x	x		x	
TG(9:0CHO_16:0_16:0)	C44H86O7N1	740.6404	x		x			
TG(9:0CHO_16:0_18:0)	C46H90O7N1	768.6717			x		x	
TG(9:0CHO_16:0_18:1)	C46H88O7N1	766.6561	x		x		x	
TG(9:0CHO_16:1_18:1)	C46 H88 O8 N1	782.6510					x	
TG(9:0CHO_18:1_18:1)	C48H90O7N1	792.6717	x	x	x	x	x	x
TG(9:0CHO_18:1_18:2)	C48H88O7N1	790.6561	x	x	x	x	x	
TG(9:0COOH_15:0_15:0)	C42H82O8N1				x			
TG(9:0COOH_16:0_16:0)	C44H86O8N1	756.6353	x				x	
TG(9:0COOH_16:0_18:1)	C46H88O8N1	782.6510	x				x	
TG(11:0CHO_16:0_18:1)	C48 H92 O7 N1	794.6874					x	
TG(11:0CHO_18:1_18:1)	C50 H94 O7 N1	820.7030					x	
Total = 34			**16**	**9**	**12**	**5**	**22**	**2**

treatment was used, meaning the cell culture medium was exposed to the plasma, and the medium was subsequently transferred to cells. While this model cannot adequately reflect the short-lived species acting on the skin, it nevertheless gives an impression of how skin cells *in vitro* respond to more complex mixtures of plasma-derived ROS. For the kINPen, these mixtures contain, for instance, hydrogen peroxide, nitrite, nitrate, or hypochlorous acid [50,51], while some short-lived species such as hydroxyl radicals, superoxide anion, and peroxynitrite quickly deteriorate in excess cell culture medium [52,53].

The plasma treatment of skin interfered with this complex regulatory network at different levels. Primarily, the number of regulated genes was elevated to a greater extent after longer treatment times (20 s), but the cellular effects seemed to be similar in tendency for both treatment times. Our global transcriptomic finding suggests that a specific pattern of cellular responses is triggered by the plasma-derived ROS delivery to the intact murine skin. Moreover, a correlation between treatment time and gene alterations was found in several *in vitro* studies in plasma-treated (20 s, 60 s, and 180 s) human skin cells showing a treatment time-dependent increase in expression and activity of targets of Nrf2 signaling or components of AP-1 (JUN) and MAPK pathways [54,55]. At higher treatment intensities, biomedical responses changed from stimulating to cytotoxic in non-malignant [55] and cancer cells [56–58]. Here, we identified the treatment-time dependent activation of critical genes of cell proliferation (e.g., Hippo signaling), differentiation, and cell cycle (Table S3). Similar to our findings in intact skin, the Hippo signaling pathway has become increasingly significant in wound healing as it is marked by a tinny regulation of cell proliferation and apoptosis [59]. Cadherins directly act on proliferation-promoting signal transduction [60,61]. If the cells in the tissue are firmly connected, a withdrawal from the cell cycle occurs with contact inhibition of proliferation [62–64]. Thus, a plasma-induced down-regulation of several cadherins has positive effects on cellular proliferation. Consistent with these results, beneficial plasma effects were already demonstrated in mammalian wound healing, including stimulated cell migration and proliferation [65–67], accelerated re-epithelialization, pro-inflammatory signaling, and wound healing in patients [68–71]. In our study using intact skin, a great bulk of induced or repressed genes include transcripts of junctional network and barrier function. The main question arose about how cold plasma regulates the barrier function of the skin.

Many inflammatory skin diseases are connected to altered distribution patterns and expression levels of TJ proteins at the cell-cell border of epidermal layers [38]. Particularly, down-regulation or knockout of integral membrane proteins (i.e., occludin, JAM, and claudin 1 and other isoforms) and TJ plaque protein ZO-1 belong to the clinical pictures of psoriasis vulgaris [14,72,73], atopic dermatitis [12,74], bacterial impetigo contagiosa [75], ichthyosis vulgaris [9,76], lichen planus [9], Hailey-Hailey disease [77], or systemic sclerosis [78]. These diseases might be targeted using plasma technology [3], generating exogenous ROS that penetrate into tissue [79]. We measured an increase of the oxygen saturation in the superficial but not deeper tissue layers by hyperspectral imaging (HSI). Since oxygen played a decisive role in tissue regeneration and angiogenesis [33,80], we found an increase in the hemoglobin distribution in the microcirculatory system. These findings are in line with studies investigating plasma-induced alterations in several tissue parameters [21,81–85] and angiogenetic

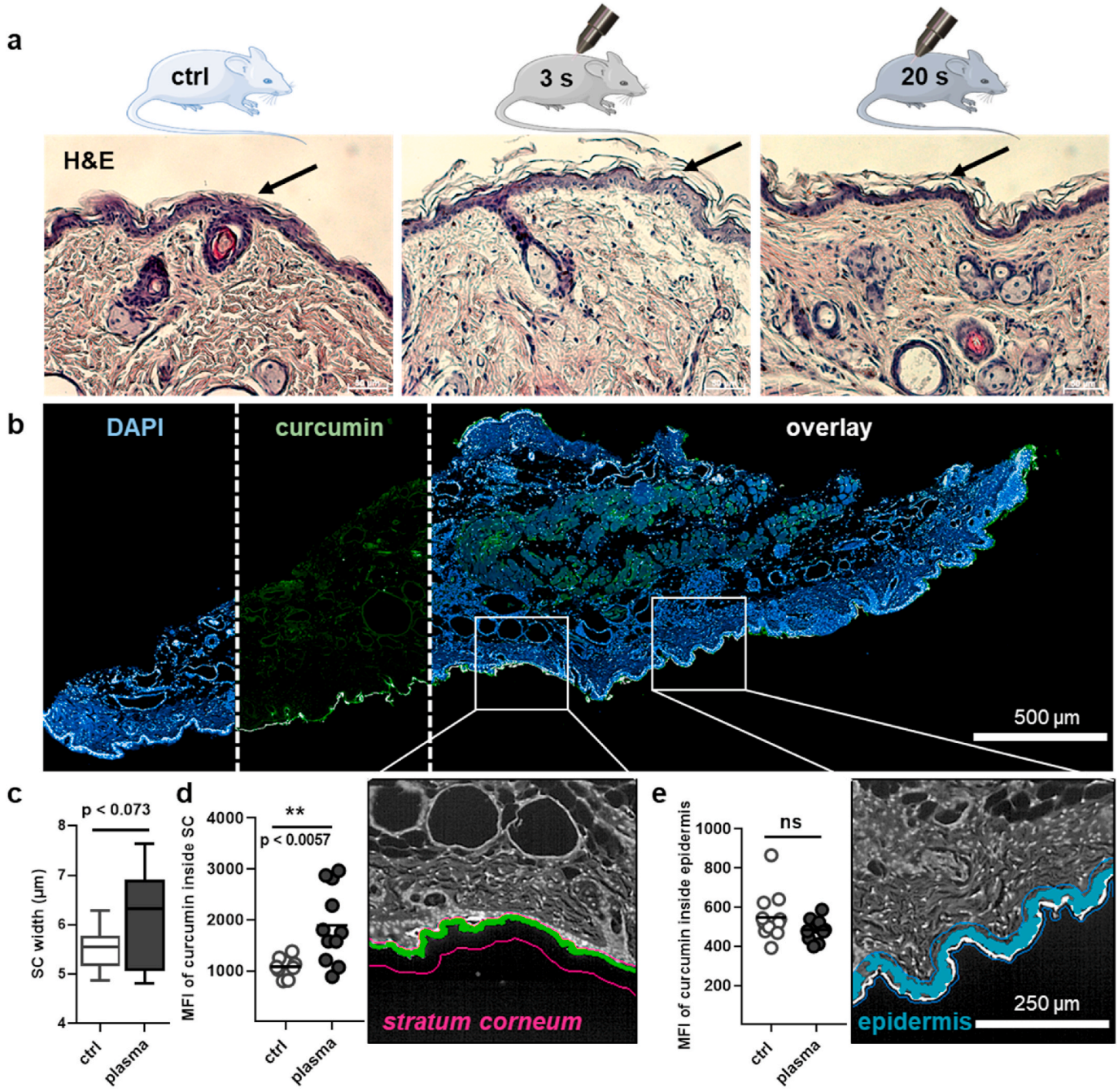

Fig. 6. Plasma treatment enhanced the accumulation of curcumin in the *stratum corneum* (SC). (a) Representative tissue sections stained with hematoxylin & eosin (H&E) in control (left), 3 s plasma-treated (middle), and 20 s plasma-treated (right) skin of mice *in vivo*. (b) Curcumin (green) and DAPI (blue) staining of a representative composite whole-section skin tissue digitally stitched from 50 individual fields of view of plasma-treated skin (3 s/mm^2). (c) Quantification of the thickness of the *stratum corneum* (SC) based on algorithm-driven high content imaging analysis of tissue sections of plasma-treated compared to untreated murine skin *in vivo*. (d–e) Quantification of curcumin staining intensity in the SC with a representative image of the SC at higher magnification showing the calculated SC image region (green, d) and in the epidermis showing the calculated epidermal image region (blue, e). Results are expressed as boxplots or individual values of several sections of 4 animals per group, and statistical analysis was performed using unpaired *t*-test with $p < 0.01$ (**). DAPI (blue in b, or greyscales in d and e) was used as nuclear counterstain. Scale bars are 50 µm (a), 500 µm (b), and 250 µm (d–e); n.s. = not significant (n = 4). (For interpretation of the references to color in this figure legend, the reader is referred to the Web version of this article.)

factors [33,86–90]. Moreover, the plasma effect on these parameters was transient and returned mostly to the baseline values in the murine skin over time, hinting to a safe medical plasma application [91–95].

In the stratified epithelia of the skin, transmembrane components of TJ, such as claudin 1, play a decisive part in skin diseases and ensure the full functionality of TJ even in the absence of occludin [78]. Claudin 1 is a permeability regulator [5,6] preventing the loss of water through the skin cells [1]. Cldn1-deficient mice do not develop an intact *stratum corneum* (SC) and lose large amounts of water through their skin [96,97]. Thus, claudin 1 can indirectly influence the skin barrier by regulating the expression of proteins that form the water-repellent layer around the SC cells. In this regard, we found a switch from an initially low to a higher value of the tissue-water content (TWI), as shown by HSI, pointing to a moderate anti-dehydration response after plasma treatment. In human volunteers, the *transepidermal water loss* (TEWL) and the moisture of the skin after plasma treatment were not changed

[98,99]. Interestingly, only claudin 1 was upregulated after plasma treatment in contrast to all other isoforms. Our observations might reflect an impairment of TJ barrier function at the time of plasma treatment, which is quickly counterbalanced by the upregulation of claudin 1, and AJ-associated E-cadherin and β-catenin in the living organism. Functional studies have fostered the hypothesis that the TJ barrier is highly dynamic [100]. This is further supported by our experimental evidence of fluctuated expression of distinct isoforms of TJ proteins and a plasma-induced balanced regulation of junctional proteins, where the spatial distribution of distinct proteins was unchanged in intact skin.

Our skin penetration experiments using the lipophilic model drug curcumin indicated that plasma treatment offers the possibility to overcome the outermost layers of the epidermis where TJ are not present. This is in line with a study where a plasma treatment yielded a regular pattern of locally permeabilized regions in the μm-range in isolated human SC [101]. The penetration of fluorescent dyes or nanocapsules could be effectively enhanced when applied in combination with plasma in the porcine ear [102–104]. However, in contrast to an *ex vivo* plasma treatment of porcine ear and human skin [105], we did not detect any permeabilization of deeper skin layers with plasma treatment. One reason may be the lipophilic nature of curcumin, which causes it to remain in the cellular lipid membrane. Another cause might be the presence of a junctional network, particularly TJ in the *stratum granulosum* (SG). Interestingly, a size dependence of paracellular flux through TJ indicates two pathways [100]. Claudins primarily regulate the pore pathway for small ions and molecules [106], while occludin appears to be essential to leak pathway regulation of larger molecules [107]. While occludin is only present in small amounts in murine skin (and was not affected by the plasma treatment), the paracellular flux of larger molecules seems to be restricted in epidermal layers. Additionally, due to the lack of changes in the permeability of the epidermis shown in occludin-deficient mice, occludin seems to play a minor role in the formation of the barrier function in murine skin [108,109]. These findings indicated a dynamic barrier regulation by a plasma-induced regulation via opening and closing events in TJ.

Via the plasma-induced disaggregation of SC cells and upregulation of claudin 1, the plasma-generated small ions and molecules presumably diffused into the epidermis and intervened in biological and biochemical processes [110,111]. Cellular signaling responses are often amplified via gap junctions (GJ) upon local stimulation to remote skin sites, not directly in contact with the initial trigger event. The GJ intercellular communication (GJIC) is ubiquitous and takes place via a network of cell junctions, receptors, and various signal molecules [8] in the dermal and epidermal skin layer [112,113]. Connexins form the GJIC channels, which allow the exchange of water, ions, and organic molecules between the epidermal cells [8]. Many different connexins are present in the skin, which are differently distributed and regulated in the individual skin layers [114,115]. Particularly Cx31 is strongly expressed in the SG [114]. Since the SG is one of the uppermost layers in the epidermis, cells are supposedly exposed to larger quantities of plasma-derived ROS, explaining the particularly strong transcriptional regulation of Cx31. Cx43 is the main connexin of the epidermis and has been described as relevant for wound healing [33,66,116]. The expression levels of Cx43 increased consistently after plasma treatment, indicating a generally increased GJIC in murine skin.

Other mechanisms by which plasma-generated ROS cross cell membrane barriers included not only a passive diffusion or the involvement of membrane channels but also through pores formed by lipid oxygenation [117]. Due to the ubiquitous distribution of lipids in cell membranes, lipids display the first contact sides and therefore targets for ROS. The oxidation of lipids results in a change of molecule size and polarity, leading to increased membrane fluidity and permeability, and hence a better penetration of ROS [118,119]. Similarly to our data, insights into lipid class diversity and lipid oxidation products were recently provided using lipids originating from the SC and sebum from 22 healthy volunteers [120]. Lipid peroxidation in the skin has also been observed by other studies discussing different oxidative targets in the SC [121–123]. SC lipids are a very diverse group, which can have two distinct origins. They can be derived from epidermal keratinocytes or secreted from sebaceous glands [124]. Sebaceous lipids are mostly nonpolar, and when secreted, they cover the skin surface as sebum. Sebum and its components have photoprotective, antimicrobial, and anti-inflammatory characteristics, and act as the first barrier against the pro-oxidative environment the skin is continuously exposed to Ref. [125]. Similar to our report, recently published data suggest that triglycerides, the most abundant sebaceous lipid class, possess a high basal oxidation level [120]. Potential further oxidation and subsequent substantial rearrangements (e.g., fragmentation and loss of fatty acids), and the formation of small secondary lipid peroxidation products such as 4-hydroxynonenal preclude their detection by our approach due to their polarity and limited suitability for electrospray ionization. Lipid oxidation was also investigated by molecular dynamics simulations showing a facilitated penetration of ROS across the SC when lipid species were oxidized by plasma [111]. In this context, also the peroxidation of triglycerides could contribute to the disaggregation of SC cells and a facilitated penetration of ROS across the SC.

Among the epidermal lipids, ceramides are most abundant and with trihydroxy- and dihydroxy ceramide subclasses identified. Ceramides are important SC components maintaining barrier function and preventing water loss due to their lamellar arrangement between corneocytes [126]. After plasma treatment, they were more abundant across all sampled layers, and ceramides with α-hydroxylated fatty acids were found to be increased. These ceramides have an amide-linked fatty acid with a hydroxyl group at the α-carbon. It may be speculated that the presence of this hydroxyl group could be a result of ROS attacking a double bond of non-hydroxylated fatty acids, yielding a naturally occurring dihydroxy ceramide. These speculations have not yet been supported by experimental evidence, and we here believe to report for the first time the oxidation of skin ceramides by externally originated ROS. Other targets (e.g., cholesterol or squalene), which could be oxidized by ROS [123], were not observed in our study due to the different experimental setup. Taken together, oxidation of triglycerides may facilitate the first entry of ROS into the SC together with an untightening of the lamellar structure of ceramides between corneocytes as observed by the increased abundance of these species on the tape strips.

Our study had limitations. First, we were not able to fully explore the temporal increase of tissue oxygenation with plasma seen after 10 min and 24 h. The strong regulation via ROS may have resulted in the release of NO and NO-dependent vasodilation, together with increased blood flow in mice [127]. The short-term effects of tissue oxygenation were attenuated after 6 h culminating in a long-term adaptation. The plasma-induced changes of the expression profile in cells and tissues are well-known and treatment time-dependent [35]. Second, while the changes of the hemoglobin concentrations suffer from poor spatial distribution in intact tissue and seem to be very low [128], a quantification of the hemoglobin concentration in homogenized tissue is difficult to standardize. However, previously we showed promotion of pro-angiogenic factors (e.g., COX2, FGF, KGF, VEGF, HBEGF, and CD31) in skin cells [55,129] in association with enhanced angiogenesis in plasma-treated tissues as shown by intravital microscopy [33,86]. Third, the temporal plasma effect on curcumin uptake into the skin was not evaluated over more extended periods. Our study design intended to address the molecular mechanisms of plasma-induced changes on barrier properties in intact skin, and understanding the long-lasting curcumin uptake may be a subject of future studies. Along similar lines, the effects of repetitive plasma treatment, as routinely done in the dermatological applications in the clinics, deserves a more profound investigation in the future. Finally, we only performed experiments in living mice, while future studies investigating living human skin would be of interest, too. Hence, our report may serve as a valuable resource for upcoming projects deciphering changes in the skin barrier properties after plasma treatment in volunteers.

4. Conclusion

Exposure to cold plasma-derived ROS enhanced skin oxygenation, perfusion, and the penetration of a lipophilic substance into the *stratum corneum*. These findings, together with a profound modulation of the tight, adherence, and gap junctional network, suggest plasma technology to be an innovative tool to modulate the barrier function of the skin. This might be of relevance for future therapy of inflammatory skin diseases or the subcutaneous penetration of substances.

5. Methods

5.1. Animal experiments and cold plasma treatment

12-weeks-old SKH1 hairless mice weighting 20–25 g (Charles River Laboratory, Sulzfeld, Germany) were provided with *ad libitum* access to water and food. The local ethics committee approved all experiments (approval number 7221.3-1.1-044/16). Cold plasma treatment was done using high-purity argon gas (Air Liquide, Paris, France) at five standard liters per minute using the atmospheric pressure argon plasma jet kINPen Med (neoplas tools, Greifswald, Germany). The kINPen ionized the argon gas at a frequency of 1 MHz for generating a multitude of different components and biologically active ROS [29]. During the plasma treatment of mice, the animals were anesthetized with ketamine/xylazine. This was done not because the plasma treatment is painful but to avoid stress for the animals that would occur when manually fixing the mice. Plasma treatment was carried out using the tip of the plasma effluent at a constant distance of 8 mm using an autoclavable spacer on different areas of the back skin. For expression analyses and hyperspectral imaging, a short (3 s/mm^2) and long (20 s/mm^2) plasma exposure was performed on separate areas and compared to untreated control areas (n = 9). For lipidomics and penetration experiments, short plasma treatment of 3 s/mm^2 was carried out (n ≥ 3).

5.2. Cell and skin sample preparation

The *in vitro* experiments were performed using primary keratinocytes isolated from the murine skin tissue (n = 10) after digestion of the epidermal layer according to recommendations of a commercially available epidermis dissociation kit. Briefly, the cell suspension was homogenized in gentleMACS C tubes using an OctaMACS dissociator for obtaining live cells filtered through 70 μm MACS SmartStrainers (Miltenyi Biotec, Bergisch-Gladbach, Germany). Cells were cultured over 10 days in keratinocytes growth medium (PromoCell, Heidelberg, Germany) in a humidified incubator at 37 °C with 5% CO_2. For the experiments, early passages from 1 to 5 were used, and the cell culture medium was changed every 2–3 days. 5 mL of Roswell Park Memorial Institute 1640 medium (RPMI; Pan Biotech, Aidenbach, Germany) supplemented with 10% fetal bovine serum, 2% glutamine, and 1% penicillin and streptomycin (Sigma, Steinheim, Germany) were plasma-treated for 60 s and added to the keratinocytes for 1 h, 6 h, and 24 h post-exposure time for subsequent downstream analyses. After 2 h, the cell culture medium was exchanged.

Twenty-four hours after plasma treatment, the animals were euthanized by cervical dislocation, and the skin tissue was removed. The tissue samples for RNA and protein analysis were transferred directly into liquid nitrogen and stored at -80 °C until homogenization. Skin samples from mice were homogenized using a high-speed FastPrep-24 5G homogenizer (MP biomedicals, Heidelberg, Germany) for obtaining lysates by using adequate buffers, lysis matrix tubes, and centrifugation at 11000 x g for 10 min at 4 °C. Tissue samples for RNA were homogenized in lysis matrix tube A with 400 μl lysis buffer from the RNA Mini Kit, tissue samples for proteins were homogenized in lysis matrix tube D with 400 μl RIPA buffer. Homogenization was carried out in three to six cycles on dry ice, each lasting 30 s. At the end of the cycles, the tissue samples were centrifuged at 4 °C and 500 g for 10 min, and the lysates were stored at -80 °C. For normalization purposes, total protein content was measured in tissue homogenates [130,131]. The samples for histology were placed in 4% paraformaldehyde for further processing.

5.3. Global transcriptomic gene expression analysis

Total RNA was isolated using the Mini RNA purification kit (Bio& Sell). The RNA extracts were treated with RNase-free DNase I to remove contaminating DNA, quantified on a spectrophotometer (Nanodrop 2000; ThermoScientific, Dreieich, Germany), analyzed for RIN number in a Bioanalyzer (Agilent, Waldbronn, Germany), and stored at -80 °C. Sample preparation and hybridization were performed according to a single-color microarray-based gene expression analysis protocol (n = 9). Briefly, for calibration, the spike-in mix was added to 100 ng of RNA, the RNA was transcribed into complementary DNA (cDNA) and amplified using the Low Input Quick Amp Labeling One Color. Subsequently, the cDNA was transcribed into complementary RNA under the incorporation of the fluorescent dye cyanine 3 (Cy3). After purification, the Cy3-cRNA was fragmented and hybridized on the microarray chip using the Gene Expression Hybridization Kit (customized 8x60K microarray chip; OakLabs, Berlin, Germany) 17 h at 65 °C. The chips were then washed using the Gene Expression Wash Buffer Kit (all from Agilent, Waldbronn, Germany), dried, and scanned using an Agilent SureScan device. The scan data were extracted using Agilent's Feature Extraction Software and analyzed by the GeneSpring software (Agilent Technologies, Santa Clara, CA, USA). The differential gene expression of the plasma-treated animals was examined in comparison to untreated control skin samples. Microarrays of nine animals per group were examined. All genes with significantly different expression ($p \leq 0.05$) and a fold-change of at least two were considered. Analysis of the genes' function was done using Gene Ontology (GO) pathway analysis and the *Protein Analysis Through Evolutionary Relationships* (PANTHER) classification system (open database).

5.4. Analysis of barrier function parameters using qPCR and western blotting

Total RNA (1 μg) in a total volume of 20 μl was reverse-transcribed, and qPCR was done using a QuantStudio 1 device (Thermo Fisher Scientific, Waltham, MA, USA). The -3-phosphate dehydrogenase (*GAPDH*) was used as a housekeeping gene and normalization control [132], which was used in numerous plasma studies [33,129,133,134]. The primers for qPCR were summarized in Table S1. Cycling parameters were: 95 °C for 1 min to activate the DNA polymerase, then 40 cycles of denaturation for 10 s at 95 °C, annealing for 15 s at 60 °C, and extension for 20 s at 72 °C. Single product formation was confirmed by melting point analysis. Samples were run in duplicate, and the $_{\Delta\Delta}$CT method was applied for statistical analysis of the CT-values. The relative gene expression levels of the plasma-treated samples were standardized to those measured in the untreated control samples (n ≥ 4).

Proteins were lysed in RIPA buffer containing protease and phosphatase inhibitors (cOmplete Mini, phosSTOP, PMSF, Sigma-Aldrich, Traunstein, Germany). Protein expression levels of claudin 1, occludin, E-cadherin, β-catenin, keratin 1/14 were determined using corresponding antibodies (Cell signaling, Frankfurt/Main, Germany) and the protein simple WES system according to the manufacturer's instructions. Band intensities were quantified using Compass for Simple Western Software, normalized to housekeeping control (GAPDH), and expressed as fold change compared to the corresponding untreated control (n ≥ 4).

5.5. Immunofluorescence and H&E staining of tissues

Fixed skin samples were embedded in paraffin and sectioned (5 μm).

Histological evaluation was made using hematoxylin and eosin (H&E) staining that highlights characteristics of the skin. For immunofluorescence staining, sections were deparaffinized, rehydrated, and immersed in 15 mmol/L citrate buffer (pH 6.0). For staining of cells in *in vitro* experiments, keratinocytes were grown on glass coverslips in keratinocytes medium until confluence (n ≥ 4). Tissues and cells on slides were subjected to permeabilization using 0.25% Triton X-100 in phosphate-buffered saline (PBS). After washing with PBS, the slides were incubated with 3% BSA solution for 30 min to block non-specific protein binding. The sections were then incubated with primary monoclonal antibodies targeted against occludin, claudin 1, ZO-1, the connexins 31 and 43, or the keratins 1 and 14 (all 1:100; Santa Cruz, Dallas, TX, USA) for 2 h at room temperature in a humid chamber. After washing, secondary anti-rabbit antibodies conjugated to Alexa Fluor 594 (Sigma, Steinheim, Germany) were added for 1 h at room temperature, followed by washing and staining with FITC-phalloidin for staining the actin cytoskeleton. Slides and cells were counterstained with 5 μM of DAPI for 20 min and mounted with Fluoromount Aqueous mounting medium (Sigma-Aldrich, Taufkirchen, Germany). Fluorescence microscopy was done using an Axio Observer Z1 (Zeiss Jena, Oberkochen, Germany). Negative controls were done by omitting the primary antibody.

5.6. Scrape loading/dye transfer in keratinocytes

The scrape loading/dye transfer (SLDT) assay was done to identify functional cell-cell communication in GJ (n ≥ 4). After different incubation periods between 15 min, 1 h, and 24 h of the plasma-treated keratinocytes, the medium was removed and replaced with 0.05% Lucifer Yellow (L0259; Sigma-Aldrich, Taufkirchen, Germany) and 0.1% dextran conjugated Texas Red (TR-Dx, 10,000 MW, D-1828; Invitrogen, Darmstadt, Germany) dissolved in PBS. A scrape across the cells was made and incubated with the fluorescent markers for 2 min to allow dye uptake by the damaged cells along the scratched site. If functional GJs connect the cells, the GJ-permeable LY diffuses to adjacent cells. The GJ-impermeable TR-Dx remains only in the damaged cells and serves as a loading control to exclude dye uptake due to the plasma treatment or dead cells only. Afterward, cells were rinsed with PBS, fixed in 4% paraformaldehyde, and observed using fluorescence microscopy (Axio Observer Z1; Zeiss Jena, Oberkochen, Germany).

5.7. Hyperspectral imaging (HSI) using TIVITA tissue camera system

The HSI camera system TIVITA Tissue (Diaspective Vision, Pepelow, Germany) was used to measure the chemical parameters under standardized conditions in real-time across a range of wavelengths of 500–1000 nm. The parameters that can be acquired by HSI spectra via software algorithms include tissue oxygenation (StO_2) in superficial layers, the perfusion into deeper skin regions of 4–6 mm (near-infrared index, NIR), the tissue hemoglobin index (THI) with monitoring of the percentage volume of hemoglobin, and the tissue water index (TWI) [85]. The working distance from the camera to the mouse skin was 50 cm. The measurements started with a baseline analysis of skin before plasma treatment to determine the background levels. HSI parameters were then assessed 10 min (0.17 h), 6 h, and 24 h after plasma treatment and compared to that of untreated controls (n = 4). The camera-specific software TIVITA Suite calculates parameters in indicated areas (quadrat).

5.8. Collection of SC samples by tape stripping and lipid extraction

After plasma (3 s/mm^2) or control treatment (n = 4) Corneofix F 20 tape strips (2.0 x 1.95 cm; Courage + Khazaka Electronic, Cologne, Germany) were placed onto the sampling area with a tweezer, pressed with light pressure onto the surface for 5 s with two fingers and stored in reaction tubes until sample workup (n = 3). In total, 9 layers were sampled. Lipids were extracted as previously described in with small modifications [135]. In brief, 900 μL methanol and 5 μL EquiSPLASH internal standard (Avanti Polar Lipids, Alabaster, AL, USA) were pipetted into the reaction tube. The solution was sonicated in an ice bath for 10 min and incubated afterward for 1 h at 4 °C and 1400 rpm in a thermomixer (Eppendorf, Wesseling-Berzdorf, Germany). Lipid extracts from three layers were combined and dried by nitrogen flow. The lipid film was rehydrated with 5 mM ammonium formate in chloroform/methanol/isopropanol (1:2:4, v/v/v) and stored at -20 °C before mass spectrometry analysis.

5.9. Reversed-phase liquid-chromatography/mass spectrometry (RP-LC/MS^2)

Lipid extracts were separated on a Vanquish UHPLC equipped with an AccuCore C30 column and precolumn (10 x 2.1 mm and 150 x 2.1 mm, 2.6 μm, ThermoFisher Scientific, Dreieich, Germany). Acetonitrile/water (A, 60:40 v/v) and isopropanol/acetonitrile (B, 90:10 v/v) were adjusted with 0.1% formic acid and 10 mM ammonium formate and used for a 31 min segmented gradient at a flow rate of 350 μL/: initial (30% B), 0.0–3.0 min (hold 30% B), 3.0–8.0 min (30–43% B), 8.0–8.1 min (43–50% B), 8.1–17.0 min (50–70% B), 17.0–24.0 (70–99% B), 24.0–27.0 (hold 99%), 27.0–27.1 (99-30% B), 27.1–31.0 (hold 30% B). Samples (3 μL) were injected twice for each polarity. The LC was coupled to a QExactive Plus high-resolution mass spectrometer (ThermoFisher Scientific, Dreieich, Germany) equipped with an Ion Max Ion source with a HESI-II probe. The following electrospray settings were used in positive ionization mode: sheath gas flow rate 14 arbitrary units (Au), aux gas flow rate 2 Au, 2.7 kV spray voltage. In negative ionization mode, the following parameters were used: 8 Au sheath gas flow rate, 3 Au aux gas flow rate, 1 Au sweep gas flow rate, 2.8 kV spray voltage. MS acquisition was performed in both polarities in data-dependent acquisition mode (DDA) with a resolving power of 70.000 at m/z 200 in the full scan mode. In MS^2, resolving power of 17.500 at m/z 200 was applied. Stepped collision energy for MS^2 fragmentation was applied from 25 to 27.

5.10. Lipidomics data analysis

The following in-built databases were used for identification: HCD, oxidized GPL, labeled GPL; GL; SP, ChE (for the deuterium-labeled internal standard), and skin lipids. The precursor tolerance was set to 5 ppm. Product tolerance was set to 8 ppm. The m-score threshold was 5%, the top-rank filter was enabled, the main node filter was set to main isomer peak, and fatty acid priority was enabled. The class and ions filter was set to “all.” The resulting lipids lists were filtered and normalized in house-build KNIME-workflow. Only lipid species identified in a minimum of two of the replicates were considered as hits. Lipids measured and identified in negative and positive ionization mode were combined after normalization, and the highest value was kept for lipids that occurred in both modes; the other value was discarded. Annotation of lipid species identified is in agreement with the nomenclature suggested in Refs. [136].

5.11. High content imaging analysis of curcumin using CLS

After plasma treatment (3 s/mm^2), the mouse skin was exposed to curcumin (10 μl/cm^2 with 10 mM in ethyl acetate) for 1 h (n = 4). Skin sections were subjected to high-content imaging analysis (Operetta CLS; Perkin Elmer, Waltham, USA). Images were taken in the brightfield (BF) channel, the curcumin fluorescence channel (λ_{ex} 475 nm; λ_{em} 500–550 nm), and the DAPI fluorescence channel (λ_{ex} 365 nm; λ_{em} 430–500 nm) with a 4.8 MP sCMOS camera and a 20x (NA = 0.16) air objective (Zeiss, Jena, Germany) utilizing laser-based autofocus. The algorithm-based segmentation of the tissues and quantification of fluorescence properties was performed utilizing the *Harmony 4.9*

(Perkin Elmer, Waltham, USA) imaging and analysis software. For this, up to 50 single images were digitally stitched, and virtual images were calculated combined from autofluorescence features and fluorescence staining to allow a software-based segmentation of the tissue section areas. The software segmentation of the *stratum corneum* and the epidermal layer was done based on their morphological and fluorescence properties to allow for quantification of the sum intensity of curcumin within these layers.

5.12. Statistical analysis

Graphing and statistical analysis were performed using prism 8.42 (GraphPad Software, San Diego, CA, USA). Mean and standard errors were calculated, graphed, and statistical analysis was performed using unpaired *t*-test, Wilcoxon matched-pairs signed-rank test, or one-way analysis of variances (ANOVA) as indicated.

Declaration of competing interest

The authors have declared that no competing interest exists.

Acknowledgments

The authors gratefully acknowledge technical support by Paula Marx and Felix Niessner (INP Greifswald), and Ulrike Mäder (Dept. of Functional Genomics, Interfaculty Institute of Genetics and Functional Genomics, University Medicine Greifswald, Germany) as well as Bernhard Rauch and Markus Grube (both Institute of Pharmacology, Greifswald University Medical Center, Greifswald, Germany) for support with animal housing.

Appendix A. Supplementary data

Supplementary data to this article can be found online at https://doi.org/10.1016/j.freeradbiomed.2020.09.026.

References

[1] E. Proksch, J.M. Brandner, J.M. Jensen, The skin: an indispensable barrier, Exp. Dermatol. 17 (2008) 1063–1072, https://doi.org/10.1111/j.1600-0625.2008.00786.x.
[2] J.M. Brandner, M. Zorn-Kruppa, T. Yoshida, I. Moll, L.A. Beck, A. De Benedetto, Epidermal tight junctions in health and disease, Tissue Barriers 3 (2015) e974451, , https://doi.org/10.4161/21688370.2014.974451.
[3] P.M. Elias, Stratum corneum defensive functions: an integrated view, J. Invest. Dermatol. 125 (2005) 183–200, https://doi.org/10.1111/j.0022-202X.2005.23668.x.
[4] L. Langbein, C. Grund, C. Kuhn, S. Praetzel, J. Kartenbeck, J.M. Brandner, I. Moll, W.W. Franke, Tight junctions and compositionally related junctional structures in mammalian stratified epithelia and cell cultures derived therefrom, Eur. J. Cell Biol. 81 (2002) 419–435, https://doi.org/10.1078/0171-9335-00270.
[5] T. Otani, T.P. Nguyen, S. Tokuda, K. Sugihara, T. Sugawara, K. Furuse, T. Miura, K. Ebnet, M. Furuse, Claudins and jam-a coordinately regulate tight junction formation and epithelial polarity, J. Cell Biol. 218 (2019) 3372–3396, https://doi.org/10.1083/jcb.201812157.
[6] C.M. Niessen, Tight junctions/adherens junctions: basic structure and function, J. Invest. Dermatol. 127 (2007) 2525–2532, https://doi.org/10.1038/sj.jid.5700865.
[7] J.M. Brandner, P. Houdek, B. Husing, C. Kaiser, I. Moll, Connexins 26, 30, and 43: differences among spontaneous, chronic, and accelerated human wound healing, J. Invest. Dermatol. 122 (2004) 1310–1320, https://doi.org/10.1111/j.0022-202X.2004.22529.x.
[8] D.A. Goodenough, D.L. Paul, Gap junctions, Cold Spring Harb. Perspect. Biol. 1 (2009) a002576, https://doi.org/10.1101/cshperspect.a002576.
[9] K. Pummi, M. Malminen, H. Aho, S.L. Karvonen, J. Peltonen, S. Peltonen, Epidermal tight junctions: zo-1 and occludin are expressed in mature, developing, and affected skin and in vitro differentiating keratinocytes, J. Invest. Dermatol. 117 (2001) 1050–1058, https://doi.org/10.1046/j.0022-202x.2001.01493.x.
[10] A.I. Bachir, A.R. Horwitz, W.J. Nelson, J.M. Bianchini, Actin-based adhesion modules mediate cell interactions with the extracellular matrix and neighboring cells, Cold Spring Harb. Perspect. Biol. 9 (2017), https://doi.org/10.1101/cshperspect.a023234.
[11] N. Kirschner, P. Houdek, M. Fromm, I. Moll, J.M. Brandner, Tight junctions form a barrier in human epidermis, Eur. J. Cell Biol. 89 (2010) 839–842, https://doi.org/10.1016/j.ejcb.2010.07.010.
[12] A. De Benedetto, R. Agnihothri, L.Y. McGirt, L.G. Bankova, L.A. Beck, Atopic dermatitis: a disease caused by innate immune defects? J. Invest. Dermatol. 129 (2009) 14–30, https://doi.org/10.1038/jid.2008.259.
[13] S. Rachow, M. Zorn-Kruppa, U. Ohnemus, N. Kirschner, S. Vidal-y-Sy, P. von den Driesch, C. Bornchen, J. Eberle, M. Mildner, E. Vettorazzi, R. Rosenthal, I. Moll, J.M. Brandner, Occludin is involved in adhesion, apoptosis, differentiation and ca2 + -homeostasis of human keratinocytes: implications for tumorigenesis, PLoS One 8 (2013) e55116, , https://doi.org/10.1371/journal.pone.0055116.
[14] N. Kirschner, C. Poetzl, P. von den Driesch, E. Wladykowski, I. Moll, M.J. Behne, J.M. Brandner, Alteration of tight junction proteins is an early event in psoriasis: putative involvement of proinflammatory cytokines, Am. J. Pathol. 175 (2009) 1095–1106, https://doi.org/10.2353/ajpath.2009.080973.
[15] M.R. Prausnitz, R. Langer, Transdermal drug delivery, Nat. Biotechnol. 26 (2008) 1261–1268, https://doi.org/10.1038/nbt.1504.
[16] A. Naik, Y.N. Kalia, R.H. Guy, Transdermal drug delivery: overcoming the skin's barrier function, Pharmaceut. Sci. Technol. Today 3 (2000) 318–326, https://doi.org/10.1016/s1461-5347(00)00295-9.
[17] M.R. Prausnitz, S. Mitragotri, R. Langer, Current status and future potential of transdermal drug delivery, Nat. Rev. Drug Discov. 3 (2004) 115–124, https://doi.org/10.1038/nrd1304.
[18] M. Schafer, S. Werner, Nrf2–a regulator of keratinocyte redox signaling, Free Radic. Biol. Med. 88 (2015) 243–252, https://doi.org/10.1016/j.freeradbiomed.2015.04.018.
[19] M.A. Ndiaye, M. Nihal, G.S. Wood, N. Ahmad, Skin, reactive oxygen species, and circadian clocks, Antioxidants Redox Signal. 20 (2014) 2982–2996, https://doi.org/10.1089/ars.2013.5645.
[20] E. Maltepe, O.D. Saugstad, Oxygen in health and disease: regulation of oxygen homeostasis–clinical implications, Pediatr. Res. 65 (2009) 261–268, https://doi.org/10.1203/PDR.0b013e31818fc83f.
[21] G. Daeschlein, R. Rutkowski, S. Lutze, S. von Podewils, C. Sicher, T. Wild, H.R. Metelmann, T. von Woedkte, M. Junger, Hyperspectral imaging: innovative diagnostics to visualize hemodynamic effects of cold plasma in wound therapy, Biomed. Tech. (Berl.) (2018), https://doi.org/10.1515/bmt-2017-0085.
[22] A. Kulcke, A. Holmer, P. Wahl, F. Siemers, T. Wild, G. Daeschlein, A compact hyperspectral camera for measurement of perfusion parameters in medicine, Biomed. Tech. (Berl.) (2018), https://doi.org/10.1515/bmt-2017-0145.
[23] A. Nicolaou, S.M. Pilkington, L.E. Rhodes, Ultraviolet-radiation induced skin inflammation: dissecting the role of bioactive lipids, Chem. Phys. Lipids 164 (2011) 535–543, https://doi.org/10.1016/j.chemphyslip.2011.04.005.
[24] A.W. Borkowski, I.H. Kuo, J.J. Bernard, T. Yoshida, M.R. Williams, N.J. Hung, B.D. Yu, L.A. Beck, R.L. Gallo, Toll-like receptor 3 activation is required for normal skin barrier repair following uv damage, J. Invest. Dermatol. 135 (2015) 569–578, https://doi.org/10.1038/jid.2014.354.
[25] S. Mitra, L.N. Nguyen, M. Akter, G. Park, E.H. Choi, N.K. Kaushik, Impact of ros generated by chemical, physical, and plasma techniques on cancer attenuation, Cancers 11 (2019), https://doi.org/10.3390/cancers11071030.
[26] A. Privat-Maldonado, A. Schmidt, A. Lin, K.D. Weltmann, K. Wende, A. Bogaerts, S. Bekeschus, Ros from physical plasmas: redox chemistry for biomedical therapy, Oxid. Med. Cell. Longev. 2019 (2019) 9062098, https://doi.org/10.1155/2019/9062098.
[27] T. von Woedtke, A. Schmidt, S. Bekeschus, K. Wende, K.D. Weltmann, Plasma medicine: a field of applied redox biology, Vivo 33 (2019) 1011–1026, https://doi.org/10.21873/invivo.11570.
[28] E.A. O'Toole, Extracellular matrix and keratinocyte migration, Clin. Exp. Dermatol. 26 (2001) 525–530.
[29] S. Reuter, T. von Woedtke, K.D. Weltmann, The kinpen-a review on physics and chemistry of the atmospheric pressure plasma jet and its applications, J. Phys. D Appl. Phys. 51 (2018), https://doi.org/10.1088/1361-6463/aab3ad.
[30] K. Wende, T. von Woedtke, K.D. Weltmann, S. Bekeschus, Chemistry and biochemistry of cold physical plasma derived reactive species in liquids, Biol. Chem. 400 (2018) 19–38, https://doi.org/10.1515/hsz-2018-0242.
[31] S. Pillai, C. Oresajo, J. Hayward, Ultraviolet radiation and skin aging: roles of reactive oxygen species, inflammation and protease activation, and strategies for prevention of inflammation-induced matrix degradation - a review, Int. J. Cosmet. Sci. 27 (2005) 17–34, https://doi.org/10.1111/j.1467-2494.2004.00241.x.
[32] D.B. Graves, The emerging role of reactive oxygen and nitrogen species in redox biology and some implications for plasma applications to medicine and biology, J. Phys. D Appl. Phys. 45 (2012) 263001, https://doi.org/10.1088/0022-3727/45/26/263001.
[33] A. Schmidt, T. von Woedtke, B. Vollmar, S. Hasse, S. Bekeschus, Nrf2 signaling and inflammation are key events in physical plasma-spurred wound healing, Theranostics 9 (2019) 1066–1084, https://doi.org/10.7150/thno.29754.
[34] A. Schmidt, K. Wende, S. Bekeschus, L. Bundscherer, A. Barton, K. Ottmuller, K.D. Weltmann, K. Masur, Non-thermal plasma treatment is associated with changes in transcriptome of human epithelial skin cells, Free Radic. Res. 47 (2013) 577–592, https://doi.org/10.3109/10715762.2013.804623.
[35] A. Schmidt, T. von Woedtke, S. Bekeschus, Periodic exposure of keratinocytes to cold physical plasma: an in vitro model for redox-related diseases of the skin, Oxid. Med. Cell. Longev. 2016 (2016) 9816072, https://doi.org/10.1155/2016/9816072.
[36] M. Laroussi, Cold plasma in medicine and healthcare: the new frontier in low temperature plasma applications, Front. Phys. 8 (2020), https://doi.org/10.3389/fphy.2020.00074.
[37] D.R. Bickers, M. Athar, Oxidative stress in the pathogenesis of skin disease, J. Invest. Dermatol. 126 (2006) 2565–2575, https://doi.org/10.1038/sj.jid.

5700340.
[38] N. Kirschner, J.M. Brandner, Barriers and more: functions of tight junction proteins in the skin, Ann. N. Y. Acad. Sci. 1257 (2012) 158–166, https://doi.org/10.1111/j.1749-6632.2012.06554.x.
[39] K. Kramm, C. Engel, D. Grohmann, Transcription initiation factor tbp: old friend new questions, Biochem. Soc. Trans. 47 (2019) 411–423, https://doi.org/10.1042/bst20180623.
[40] E. Lasda, R. Parker, Circular rnas: diversity of form and function, RNA 20 (2014) 1829–1842, https://doi.org/10.1261/rna.047126.114.
[41] C.K. Sen, L. Packer, Antioxidant and redox regulation of gene transcription, Faseb. J. 10 (1996) 709–720, https://doi.org/10.1096/fasebj.10.7.8635688.
[42] H. Jablonowski, T. von Woedtke, Research on plasma medicine-relevant plasma–liquid interaction: what happened in the past five years? Clin. Plas. Med. 3 (2015) 42–52, https://doi.org/10.1016/j.cpme.2015.11.003.
[43] A. Dzimitrowicz, A. Bielawska-Pohl, P. Jamroz, J. Dora, A. Krawczenko, G. Busco, C. Grillon, C. Kieda, A. Klimczak, D. Terefinko, A. Baszczynska, P. Pohl, Activation of the normal human skin cells by a portable dielectric barrier discharge-based reaction-discharge system of a defined gas temperature, Plasma Chem. Plasma Process. 40 (2019) 79–97, https://doi.org/10.1007/s11090-019-10039-0.
[44] F. Girard, M. Peret, N. Dumont, V. Badets, S. Blanc, K. Gazeli, C. Noel, T. Belmonte, L. Marlin, J.P. Cambus, et al., Correlations between gaseous and liquid phase chemistries induced by cold atmospheric plasmas in a physiological buffer, Phys. Chem. Chem. Phys. 20 (2018) 9198–9210, https://doi.org/10.1039/C8CP00264A.
[45] Y. Gorbanev, A. Privat-Maldonado, A. Bogaerts, Analysis of short-lived reactive species in plasma-air-water systems: the dos and the do nots, Anal. Chem. (2018), https://doi.org/10.1021/acs.analchem.8b03336.
[46] A. Schmidt-Bleker, R. Bansemer, S. Reuter, K.-D. Weltmann, How to produce an nox- instead of ox-based chemistry with a cold atmospheric plasma jet, Plasma Process. Polym. 13 (2016) 1120–1127, https://doi.org/10.1002/ppap.201600062.
[47] W.O. Ji, M.H. Lee, G.H. Kim, E.H. Kim, Quantitation of the ros production in plasma and radiation treatments of biotargets, Sci. Rep. 9 (2019) 19837, https://doi.org/10.1038/s41598-019-56160-0.
[48] F. Girard, V. Badets, S. Blanc, K. Gazeli, L. Marlin, L. Authier, P. Svarnas, N. Sojic, F. Clement, S. Arbault, Formation of reactive nitrogen species including peroxynitrite in physiological buffer exposed to cold atmospheric plasma, RSC Adv. 6 (2016) 78457–78467, https://doi.org/10.1039/c6ra12791f.
[49] H. Jablonowski, J. Santos Sousa, K.D. Weltmann, K. Wende, S. Reuter, Quantification of the ozone and singlet delta oxygen produced in gas and liquid phases by a non-thermal atmospheric plasma with relevance for medical treatment, Sci. Rep. 8 (2018) 12195, https://doi.org/10.1038/s41598-018-30483-w.
[50] S. Bekeschus, C.C. Winterbourn, J. Kolata, K. Masur, S. Hasse, B.M. Broker, H.A. Parker, Neutrophil extracellular trap formation is elicited in response to cold physical plasma, J. Leukoc. Biol. 100 (2016) 791–799, https://doi.org/10.1189/jlb.3A0415-165RR.
[51] E. Freund, K.R. Liedtke, J. van der Linde, H.R. Metelmann, C.D. Heidecke, L.I. Partecke, S. Bekeschus, Physical plasma-treated saline promotes an immunogenic phenotype in ct26 colon cancer cells in vitro and in vivo, Sci. Rep. 9 (2019) 634, https://doi.org/10.1038/s41598-018-37169-3.
[52] S. Bekeschus, J. Kolata, C. Winterbourn, A. Kramer, R. Turner, K.D. Weltmann, B. Broker, K. Masur, Hydrogen peroxide: a central player in physical plasma-induced oxidative stress in human blood cells, Free Radic. Res. 48 (2014) 542–549, https://doi.org/10.3109/10715762.2014.892937.
[53] S. Bekeschus, A. Schmidt, F. Niessner, T. Gerling, K.D. Weltmann, K. Wende, Basic research in plasma medicine - a throughput approach from liquids to cells, J Vis Exp e56331 (2017), https://doi.org/10.3791/56331.
[54] A. Schmidt, S. Dietrich, A. Steuer, K.D. Weltmann, T. von Woedtke, K. Masur, K. Wende, Non-thermal plasma activates human keratinocytes by stimulation of antioxidant and phase ii pathways, J. Biol. Chem. 290 (2015) 6731–6750, https://doi.org/10.1074/jbc.M114.603555.
[55] A. Schmidt, S. Bekeschus, K. Jarick, S. Hasse, T. von Woedtke, K. Wende, Cold physical plasma modulates p53 and mitogen-activated protein kinase signaling in keratinocytes, Oxid. Med. Cell. Longev. 2019 (2019) 1–16, https://doi.org/10.1155/2019/7017363.
[56] S. Bekeschus, R. Clemen, F. Niessner, S.K. Sagwal, E. Freund, A. Schmidt, Medical gas plasma jet technology targets murine melanoma in an immunogenic fashion, Adv. Sci. 7 (2020) 1903438, https://doi.org/10.1002/advs.201903438.
[57] T. Bernhardt, M.L. Semmler, M. Schafer, S. Bekeschus, S. Emmert, L. Boeckmann, Plasma medicine: applications of cold atmospheric pressure plasma in dermatology, Oxid. Med. Cell. Longev. 2019 (2019) 3873928, https://doi.org/10.1155/2019/3873928.
[58] S. Bekeschus, S. Eisenmann, S.K. Sagwal, Y. Bodnar, J. Moritz, B. Poschkamp, I. Stoffels, S. Emmert, M. Madesh, K.D. Weltmann, T. von Woedtke, R.K. Gandhirajan, Xct (slc7a11) expression confers intrinsic resistance to physical plasma treatment in tumor cells, Redox Biol. 30 (2020) 101423, https://doi.org/10.1016/j.redox.2019.101423.
[59] D. Shome, T. von Woedtke, K. Riedel, K. Masur, The hippo transducer yap and its targets ctgf and cyr61 drive a paracrine signalling in cold atmospheric plasma-mediated wound healing, Oxid. Med. Cell. Longev. (2020) 1–14, https://doi.org/10.1155/2020/4910280 2020.
[60] M.L. Mucenski, J.M. Nation, A.R. Thitoff, V. Besnard, Y. Xu, S.E. Wert, N. Harada, M.M. Taketo, M.T. Stahlman, J.A. Whitsett, Beta-catenin regulates differentiation of respiratory epithelial cells in vivo, Am. J. Physiol. Lung Cell Mol. Physiol. 289 (2005) L971–L979, https://doi.org/10.1152/ajplung.00172.2005.
[61] B.T. MacDonald, K. Tamai, X. He, Wnt/beta-catenin signaling: components, mechanisms, and diseases, Dev. Cell 17 (2009) 9–26, https://doi.org/10.1016/j.devcel.2009.06.016.
[62] M. Perrais, X. Chen, M. Perez-Moreno, B.M. Gumbiner, E-cadherin homophilic ligation inhibits cell growth and epidermal growth factor receptor signaling independently of other cell interactions, Mol. Biol. Cell 18 (2007) 2013–2025, https://doi.org/10.1091/mbc.e06-04-0348.
[63] H. Eagle, E.M. Levine, Growth regulatory effects of cellular interaction, Nature 213 (1967) 1102–1106, https://doi.org/10.1038/2131102a0.
[64] A.I. McClatchey, A.S. Yap, Contact inhibition (of proliferation) redux, Curr. Opin. Cell Biol. 24 (2012) 685–694, https://doi.org/10.1016/j.ceb.2012.06.009.
[65] T. von Woedtke, S. Reuter, K. Masur, K.D. Weltmann, Plasmas for medicine, Phys. Rep. 530 (2013) 291–320, https://doi.org/10.1016/j.physrep.2013.05.005.
[66] A. Schmidt, S. Bekeschus, K. Wende, B. Vollmar, T. von Woedtke, A cold plasma jet accelerates wound healing in a murine model of full-thickness skin wounds, Exp. Dermatol. 26 (2017) 156–162, https://doi.org/10.1111/exd.13156.
[67] S. Hasse, T. Duong Tran, O. Hahn, S. Kindler, H.R. Metelmann, T. von Woedtke, K. Masur, Induction of proliferation of basal epidermal keratinocytes by cold atmospheric-pressure plasma, Clin. Exp. Dermatol. 41 (2016) 202–209, https://doi.org/10.1111/ced.12735.
[68] J. Heinlin, J.L. Zimmermann, F. Zeman, W. Bunk, G. Isbary, M. Landthaler, T. Maisch, R. Monetti, G. Morfill, T. Shimizu, J. Steinbauer, W. Stolz, S. Karrer, Randomized placebo-controlled human pilot study of cold atmospheric argon plasma on skin graft donor sites, Wound Repair Regen. 21 (2013) 800–807, https://doi.org/10.1111/wrr.12078.
[69] G. Isbary, T. Shimizu, J.L. Zimmermann, J. Heinlin, S. Al-Zaabi, M. Rechfeld, G.E. Morfill, S. Karrer, W. Stolz, Randomized placebo-controlled clinical trial showed cold atmospheric argon plasma relieved acute pain and accelerated healing in herpes zoster, Clin. Plas. Med. 2 (2014) 50–55, https://doi.org/10.1016/j.cpme.2014.07.001.
[70] H.-R. Metelmann, T.T. Vu, H.T. Do, T.N.B. Le, T.H.A. Hoang, T.T.T. Phi, T.M.L. Luong, V.T. Doan, T.T.H. Nguyen, T.H.M. Nguyen, et al., Scar formation of laser skin lesions after cold atmospheric pressure plasma (cap) treatment: a clinical long term observation, Clin. Plas. Med. 1 (2013) 30–35, https://doi.org/10.1016/j.cpme.2012.12.001.
[71] B. Stratmann, T.C. Costea, C. Nolte, J. Hiller, J. Schmidt, J. Reindel, K. Masur, W. Motz, J. Timm, W. Kerner, D. Tschoepe, Effect of cold atmospheric plasma therapy vs standard therapy placebo on wound healing in patients with diabetic foot ulcers: a randomized clinical trial, JAMA Netw. Open 3 (2020) e2010411, , https://doi.org/10.1001/jamanetworkopen.2020.10411.
[72] S. Peltonen, J. Riehokainen, K. Pummi, J. Peltonen, Tight junction components occludin, zo-1, and claudin-1, -4 and -5 in active and healing psoriasis, Br. J. Dermatol. 156 (2007) 466–472, https://doi.org/10.1111/j.1365-2133.2006.07642.x.
[73] R.E. Watson, R. Poddar, J.M. Walker, I. McGuill, L.M. Hoare, C.E. Griffiths, C.A. O'Neill, Altered claudin expression is a feature of chronic plaque psoriasis, J. Pathol. 212 (2007) 450–458, https://doi.org/10.1002/path.2200.
[74] A. De Benedetto, N.M. Rafaels, L.Y. McGirt, A.I. Ivanov, S.N. Georas, C. Cheadle, A.E. Berger, K. Zhang, S. Vidyasagar, T. Yoshida, et al., Tight junction defects in patients with atopic dermatitis, J. Allergy Clin. Immunol. 127 (2011) 773–786, https://doi.org/10.1016/j.jaci.2010.10.018 e771-777.
[75] U. Ohnemus, K. Kohrmeyer, P. Houdek, H. Rohde, E. Wladykowski, S. Vidal, M.A. Horstkotte, M. Aepfelbacher, N. Kirschner, M.J. Behne, I. Moll, J.M. Brandner, Regulation of epidermal tight-junctions (tj) during infection with exfoliative toxin-negative staphylococcus strains, J. Invest. Dermatol. 128 (2008) 906–916, https://doi.org/10.1038/sj.jid.5701070.
[76] R. Gruber, P.M. Elias, D. Crumrine, T.K. Lin, J.M. Brandner, J.P. Hachem, R.B. Presland, P. Fleckman, A.R. Janecke, A. Sandilands, et al., Filaggrin genotype in ichthyosis vulgaris predicts abnormalities in epidermal structure and function, Am. J. Pathol. 178 (2011) 2252–2263, https://doi.org/10.1016/j.ajpath.2011.01.053.
[77] L. Raiko, P. Leinonen, P.M. Hagg, J. Peltonen, A. Oikarinen, S. Peltonen, Tight junctions in hailey-hailey and darier's diseases, Dermatol. Rep. 1 (2009) e1, https://doi.org/10.4081/dr.2009.e1.
[78] Y. Hou, B.J. Rabquer, M.L. Gerber, F. Del Galdo, S.A. Jimenez, G.K. Haines 3rd, W.G. Barr, M.C. Massa, J.R. Seibold, A.E. Koch, Junctional adhesion molecule-a is abnormally expressed in diffuse cutaneous systemic sclerosis skin and mediates myeloid cell adhesion, Ann. Rheum. Dis. 69 (2010) 249–254, https://doi.org/10.1136/ard.2008.102624.
[79] T. Kawasaki, A. Sato, S. Kusumegi, A. Kudo, T. Sakanoshita, T. Tsurumaru, G. Uchida, K. Koga, M. Shiratani, Two-dimensional concentration distribution of reactive oxygen species transported through a tissue phantom by atmospheric-pressure plasma-jet irradiation, APEX 9 (2016) 076202, , https://doi.org/10.7567/Apex.9.076202.
[80] D.M. Castilla, Z.J. Liu, O.C. Velazquez, Oxygen: implications for wound healing, Adv. Wound Care 1 (2012) 225–230, https://doi.org/10.1089/wound.2011.0319.
[81] T. Kisch, S. Schleusser, A. Helmke, K.L. Mauss, E.T. Wenzel, B. Hasemann, P. Mailaender, R. Kraemer, The repetitive use of non-thermal dielectric barrier discharge plasma boosts cutaneous microcirculatory effects, Microvasc. Res. 106 (2016) 8–13, https://doi.org/10.1016/j.mvr.2016.02.008.
[82] T. Borchardt, J. Ernst, A. Helmke, M. Tanyeli, A.F. Schilling, G. Felmerer, W. Viol, Effect of direct cold atmospheric plasma (dicap) on microcirculation of intact skin in a controlled mechanical environment, Microcirculation 24 (2017), https://doi.org/10.1111/micc.12399.
[83] R. Rutkowski, M. Schuster, J. Unger, C. Seebauer, H.R. Metelmann, T.v. Woedtke, K.D. Weltmann, G. Daeschlein, Hyperspectral imaging for in vivo monitoring of cold atmospheric plasma effects on microcirculation in treatment of head and neck

cancer and wound healing, Clin. Plas. Med. 7–8 (2017) 52–57, https://doi.org/10.1016/j.cpme.2017.09.002.
[84] M. Wahabzada, M. Besser, M. Khosravani, M.T. Kuska, K. Kersting, A.K. Mahlein, E. Sturmer, Monitoring wound healing in a 3d wound model by hyperspectral imaging and efficient clustering, PLoS One 12 (2017) e0186425, , https://doi.org/10.1371/journal.pone.0186425.
[85] A. Schmidt, F. Niessner, T. von Woedtke, S. Bekeschus, Hyperspectral imaging of wounds reveals augmented tissue oxygenation following cold physical plasma treatment in vivo, IEEE Trans. Radiat. Plasma Med. Sci. (2020), https://doi.org/10.1109/trpms.2020.3009913 1-1.
[86] S. Arndt, A. Schmidt, S. Karrer, T. von Woedtke, Comparing two different plasma devices kinpen and adtec steriplas regarding their molecular and cellular effects on wound healing, Clin. Plas. Med. 9 (2018) 24–33, https://doi.org/10.1016/j.cpme.2018.01.002.
[87] M. Chatraie, G. Torkaman, M. Khani, H. Salehi, B. Shokri, In vivo study of non-invasive effects of non-thermal plasma in pressure ulcer treatment, Sci. Rep. 8 (2018) 5621, https://doi.org/10.1038/s41598-018-24049-z.
[88] G. Lloyd, G. Friedman, S. Jafri, G. Schultz, A. Fridman, K. Harding, Gas plasma: medical uses and developments in wound care, Plasma Process. Polym. 7 (2010) 194–211, https://doi.org/10.1002/ppap.200900097.
[89] M.-H. Ngo Thi, P.-L. Shao, J.-D. Liao, C.-C.K. Lin, H.-K. Yip, Enhancement of angiogenesis and epithelialization processes in mice with burn wounds through ros/rns signals generated by non-thermal n2/ar micro-plasma, Plasma Process. Polym. 11 (2014) 1076–1088, https://doi.org/10.1002/ppap.201400072.
[90] K. Priya Arjunan, A. Morss Clyne, Hydroxyl radical and hydrogen peroxide are primarily responsible for dielectric barrier discharge plasma-induced angiogenesis, Plasma Process. Polym. 8 (2011) 1154–1164, https://doi.org/10.1002/ppap.201100078.
[91] J. Heinlin, G. Isbary, W. Stolz, F. Zeman, M. Landthaler, G. Morfill, T. Shimizu, J.L. Zimmermann, S. Karrer, A randomized two-sided placebo-controlled study on the efficacy and safety of atmospheric non-thermal argon plasma for pruritus, J. Eur. Acad. Dermatol. Venereol. 27 (2013) 324–331, https://doi.org/10.1111/j.1468-3083.2011.04395.x.
[92] G. Isbary, J. Köritzer, A. Mitra, Y.F. Li, T. Shimizu, J. Schroeder, J. Schlegel, G.E. Morfill, W. Stolz, J.L. Zimmermann, Ex vivo human skin experiments for the evaluation of safety of new cold atmospheric plasma devices, Clin. Plas. Med. 1 (2013) 36–44, https://doi.org/10.1016/j.cpme.2012.10.001.
[93] L. Jablonowski, T. Kocher, A. Schindler, K. Muller, F. Dombrowski, T. von Woedtke, T. Arnold, A. Lehmann, S. Rupf, M. Evert, K. Evert, Side effects by oral application of atmospheric pressure plasma on the mucosa in mice, PLoS One 14 (2019) e0215099, , https://doi.org/10.1371/journal.pone.0215099.
[94] D.H. Xu, Q.J. Cui, Y.J. Xu, B.C. Wang, M. Tian, Q.S. Li, Z.J. Liu, D.X. Liu, H.L. Chen, M.G. Kong, Systemic study on the safety of immuno-deficient nude mice treated by atmospheric plasma-activated water, Plasma Sci. Technol. 20 (2018), https://doi.org/10.1088/2058-6272/aa9842.
[95] A. Schmidt, T.V. Woedtke, J. Stenzel, T. Lindner, S. Polei, B. Vollmar, S. Bekeschus, One year follow-up risk assessment in skh-1 mice and wounds treated with an argon plasma jet, Int. J. Mol. Sci. 18 (2017), https://doi.org/10.3390/ijms18040868.
[96] N. Kirschner, R. Rosenthal, M. Furuse, I. Moll, M. Fromm, J.M. Brandner, Contribution of tight junction proteins to ion, macromolecule, and water barrier in keratinocytes, J. Invest. Dermatol. 133 (2013) 1161–1169, https://doi.org/10.1038/jid.2012.507.
[97] S. Tsukita, M. Furuse, Claudin-based barrier in simple and stratified cellular sheets, Curr. Opin. Cell Biol. 14 (2002) 531–536, https://doi.org/10.1016/s0955-0674(02)00362-9.
[98] G. Daeschlein, S. Scholz, R. Ahmed, A. Majumdar, T. von Woedtke, H. Haase, M. Niggemeier, E. Kindel, R. Brandenburg, K.D. Weltmann, M. Junger, Cold plasma is well-tolerated and does not disturb skin barrier or reduce skin moisture, J. Dtsch. Dermatol. Ges 10 (2012) 509–515, https://doi.org/10.1111/j.1610-0387.2012.07857.x.
[99] J.W. Fluhr, S. Sassning, O. Lademann, M.E. Darvin, S. Schanzer, A. Kramer, H. Richter, W. Sterry, J. Lademann, In vivo skin treatment with tissue-tolerable plasma influences skin physiology and antioxidant profile in human stratum corneum, Exp. Dermatol. 21 (2012) 130–134, https://doi.org/10.1111/j.1600-0625.2011.01411.x.
[100] C.R. Weber, Dynamic properties of the tight junction barrier, Ann. N. Y. Acad. Sci. 1257 (2012) 77–84, https://doi.org/10.1111/j.1749-6632.2012.06528.x.
[101] M. Gelker, C.C. Müller-Goymann, W. Viöl, Permeabilization of human stratum corneum and full-thickness skin samples by a direct dielectric barrier discharge, Clin. Plas. Med. 9 (2018) 34–40, https://doi.org/10.1016/j.cpme.2018.02.001.
[102] J. Lademann, A. Patzelt, H. Richter, O. Lademann, G. Baier, L. Breucker, K. Landfester, Nanocapsules for drug delivery through the skin barrier by tissue-tolerable plasma, Laser Phys. Lett. 10 (2013) 083001, , https://doi.org/10.1088/1612-2011/10/8/083001.
[103] O. Lademann, H. Richter, A. Kramer, A. Patzelt, M.C. Meinke, C. Graf, Q. Gao, E. Korotianskiy, E. Rühl, K.D. Weltmann, J. Lademann, S. Koch, Stimulation of the penetration of particles into the skin by plasma tissue interaction, Laser Phys. Lett. 8 (2011) 758–764, https://doi.org/10.1002/lapl.201110055.
[104] O. Lademann, H. Richter, M.C. Meinke, A. Patzelt, A. Kramer, P. Hinz, K.D. Weltmann, B. Hartmann, S. Koch, Drug delivery through the skin barrier enhanced by treatment with tissue-tolerable plasma, Exp. Dermatol. 20 (2011) 488–490, https://doi.org/10.1111/j.1600-0625.2010.01245.x.
[105] M. Gelker, Müller-Goymann, C. Christel, W. Viöl, Plasma permeabilization of human excised full-thickness skin by μs- and ns-pulsed dbd, Skin Pharmacol. Physiol. 33 (2020) 69–76, https://doi.org/10.1159/000505195.
[106] C.M. Van Itallie, J. Holmes, A. Bridges, J.L. Gookin, M.R. Coccaro, W. Proctor, O.R. Colegio, J.M. Anderson, The density of small tight junction pores varies among cell types and is increased by expression of claudin-2, J. Cell Sci. 121 (2008) 298–305, https://doi.org/10.1242/jcs.021485.
[107] A.S. Yu, K.M. McCarthy, S.A. Francis, J.M. McCormack, J. Lai, R.A. Rogers, R.D. Lynch, E.E. Schneeberger, Knockdown of occludin expression leads to diverse phenotypic alterations in epithelial cells, Am. J. Physiol. Cell Physiol. 288 (2005) C1231–C1241, https://doi.org/10.1152/ajpcell.00581.2004.
[108] G.J. Feldman, J.M. Mullin, M.P. Ryan, Occludin: structure, function and regulation, Adv. Drug Deliv. Rev. 57 (2005) 883–917, https://doi.org/10.1016/j.addr.2005.01.009.
[109] J.D. Schulzke, A.H. Gitter, J. Mankertz, S. Spiegel, U. Seidler, S. Amasheh, M. Saitou, S. Tsukita, M. Fromm, Epithelial transport and barrier function in occludin-deficient mice, Biochim. Biophys. Acta 1669 (2005) 34–42, https://doi.org/10.1016/j.bbamem.2005.01.008.
[110] J. Duan, X. Lu, G. He, On the penetration depth of reactive oxygen and nitrogen species generated by a plasma jet through real biological tissue, Phys. Plasmas 24 (2017), https://doi.org/10.1063/1.4990554.
[111] J. Duan, M. Ma, M. Yusupov, R.M. Cordeiro, X. Lu, A. Bogaerts, The penetration of reactive oxygen and nitrogen species across the stratum corneum, Plasma Process. Polym. (2020), https://doi.org/10.1002/ppap.202000005.
[112] C. Borek, S. Higashino, W.R. Loewenstein, Intercellular communication and tissue growth : iv. Conductance of membrane junctions of normal and cancerous cells in culture, J. Membr. Biol. 1 (1969) 274–293, https://doi.org/10.1007/BF01869786.
[113] D. Salomon, J.H. Saurat, P. Meda, Cell-to-cell communication within intact human skin, J. Clin. Invest. 82 (1988) 248–254, https://doi.org/10.1172/JCI113578.
[114] W.L. Di, E.L. Rugg, I.M. Leigh, D.P. Kelsell, Multiple epidermal connexins are expressed in different keratinocyte subpopulations including connexin 31, J. Invest. Dermatol. 117 (2001) 958–964, https://doi.org/10.1046/j.0022-202x.2001.01468.x.
[115] J.A. Goliger, D.L. Paul, Expression of gap junction proteins cx26, cx31.1, cx37, and cx43 in developing and mature rat epidermis, Dev. Dynam. 200 (1994) 1–13, https://doi.org/10.1002/aja.1002000102.
[116] C. Qiu, P. Coutinho, S. Frank, S. Franke, L.Y. Law, P. Martin, C.R. Green, D.L. Becker, Targeting connexin43 expression accelerates the rate of wound repair, Curr. Biol. 13 (2003) 1697–1703, https://doi.org/10.1016/j.cub.2003.09.007.
[117] E.J. Szili, S.H. Hong, J.S. Oh, N. Gaur, R.D. Short, Tracking the penetration of plasma reactive species in tissue models, Trends Biotechnol. 36 (2018) 594–602, https://doi.org/10.1016/j.tibtech.2017.07.012.
[118] K.A. Runas, N. Malmstadt, Low levels of lipid oxidation radically increase the passive permeability of lipid bilayers, Soft Matter 11 (2015) 499–505, https://doi.org/10.1039/c4sm01478b.
[119] M. Yusupov, K. Wende, S. Kupsch, E.C. Neyts, S. Reuter, A. Bogaerts, Effect of head group and lipid tail oxidation in the cell membrane revealed through integrated simulations and experiments, Sci. Rep. 7 (2017) 5761, https://doi.org/10.1038/s41598-017-06412-8.
[120] J. Striesow, J.W. Lackmann, Z. Ni, S. Wenske, K.D. Weltmann, M. Fedorova, T. von Woedtke, K. Wende, Oxidative modification of skin lipids by cold atmospheric plasma (cap): a standardizable approach using rp-lc/ms(2) and di-esi/ms(2), Chem. Phys. Lipids 226 (2020) 104786, https://doi.org/10.1016/j.chemphyslip.2019.104786.
[121] J. Lasch, U. Schönfelder, M. Walke, S. Zellmer, D. Beckert, Oxidative damage of human skin lipids, Biochim. Biophys. Acta Lipids Lipid. Metabol. 1349 (1997) 171–181, https://doi.org/10.1016/s0005-2760(97)00093-3.
[122] J.J. Thiele, Oxidative targets in the stratum corneum. A new basis for antioxidative strategies, Skin Pharmacol. Appl. Skin Physiol. 14 (Suppl 1) (2001) 87–91, https://doi.org/10.1159/000056395.
[123] E. Niki, Lipid oxidation in the skin, Free Radic. Res. 49 (2015) 827–834, https://doi.org/10.3109/10715762.2014.976213.
[124] A. Pappas, Epidermal surface lipids, Dermatoendocrinol 1 (2009) 72–76, https://doi.org/10.4161/derm.1.2.7811.
[125] M. Picardo, M. Ottaviani, E. Camera, A. Mastrofrancesco, Sebaceous gland lipids, Dermatoendocrinol 1 (2009) 68–71, https://doi.org/10.4161/derm.1.2.8472.
[126] H.J. Cha, C. He, H. Zhao, Y. Dong, I.S. An, S. An, Intercellular and intracellular functions of ceramides and their metabolites in skin (review), Int. J. Mol. Med. 38 (2016) 16–22, https://doi.org/10.3892/ijmm.2016.2600.
[127] S. Arndt, P. Unger, M. Berneburg, A.K. Bosserhoff, S. Karrer, Cold atmospheric plasma (cap) activates angiogenesis-related molecules in skin keratinocytes, fibroblasts and endothelial cells and improves wound angiogenesis in an autocrine and paracrine mode, J. Dermatol. Sci. 89 (2018) 181–190, https://doi.org/10.1016/j.jdermsci.2017.11.008.
[128] F.E. Robles, S. Chowdhury, A. Wax, Assessing hemoglobin concentration using spectroscopic optical coherence tomography for feasibility of tissue diagnostics, Biomed. Optic Express 1 (2010) 310–317, https://doi.org/10.1364/boe.1.000310/.
[129] A. Barton, K. Wende, L. Bundscherer, S. Hasse, A. Schmidt, S. Bekeschus, K.-D. Weltmann, U. Lindequist, K. Masur, Nonthermal plasma increases expression of wound healing related genes in a keratinocyte cell line, Plasma Med. 3 (2013) 125–136, https://doi.org/10.1615/PlasmaMed.2014008540.
[130] O.H. Lowry, N.J. Rosebrough, A.L. Farr, R.J. Randall, Protein measurement with the folin phenol reagent, J. Biol. Chem. 193 (1951) 265–275.
[131] G.L. Miller, Protein determination for large numbers of samples, Anal. Chem. 31 (1959), https://doi.org/10.1021/ac60149a611 964-964.
[132] H.M. Said, C. Hagemann, J. Stojic, B. Schoemig, G.H. Vince, M. Flentje, K. Roosen, D. Vordermark, Gapdh is not regulated in human glioblastoma under hypoxic conditions, BMC Mol. Biol. 8 (55) (2007), https://doi.org/10.1186/1471-2199-

8-55.
[133] M. Ghaemi, A. Majd, A. Iranbakhsh, Transcriptional responses following seed priming with cold plasma and electromagnetic field in salvia nemorosa l, J. Theor. Appl. Phys. (2020), https://doi.org/10.1007/s40094-020-00387-0.
[134] D.K. Yadav, M. Adhikari, S. Kumar, B. Ghimire, I. Han, M.H. Kim, E.H. Choi, Cold atmospheric plasma generated reactive species aided inhibitory effects on human melanoma cells: an in vitro and in silico study, Sci. Rep. 10 (2020) 3396, https://doi.org/10.1038/s41598-020-60356-0.
[135] T. Sadowski, C. Klose, M.J. Gerl, A. Wojcik-Maciejewicz, R. Herzog, K. Simons, A. Reich, M.A. Surma, Large-scale human skin lipidomics by quantitative, high-throughput shotgun mass spectrometry, Sci. Rep. 7 (2017) 43761, https://doi.org/10.1038/srep43761.
[136] G. Liebisch, J.A. Vizcaino, H. Kofeler, M. Trotzmuller, W.J. Griffiths, G. Schmitz, F. Spener, M.J. Wakelam, Shorthand notation for lipid structures derived from mass spectrometry, J. Lipid Res. 54 (2013) 1523–1530, https://doi.org/10.1194/jlr.M033506.